Available online at www.CivileJournal.org

Civil Engineering Journal

(E-ISSN: 2476-3055; ISSN: 2676-6957)

Vol. 10, No. 10, October, 2024

Analysis of Tetrachiral Sandwich Structures at High-Velocity Impact: Influence of the Applied Material and Projectile Core Geometry

Sultan Maulana [1], Aditya Rio Prabowo [1*], Wibowo Wibowo [1], Quang Thang Do [2], Teguh Muttaqie [3], Nurul Muhayat [1], Siti Nurlita Fitri [4]

[1] Department of Mechanical Engineering, Universitas Sebelas Maret, Surakarta, Indonesia.

[2] Department of Naval Architecture and Ocean Engineering, Nha Trang University, Nha Trang, Viet Nam.

[3] Research Center of Testing Technology and Standard, National Research and Innovation Agency (BRIN), Tangerang, Indonesia.

[4] Department of Civil Engineering, Gifu University, Gifu, Japan.

Received 07 June 2024; Revised 19 September 2024; Accepted 24 September 2024; Published 01 October 2024

Abstract

This research involved ballistic impact analysis on a tetrachiral sandwich structure in which the shapes of the circular nodes in the tetrachiral core are modified into polygonal shapes, namely a square, hexagon, and octagon. The objectives of this study were to observe the effect of a modified sandwich tetrachiral structure core, investigate the effect of the projectile geometry, and calculate the material performance of the structure. This research was conducted using numerical analysis utilizing the finite element method. The simulation methodology was validated through a benchmarking study, the results of which showed an error below 6%. The findings show that the material with the best performance was Armox 500T, at 5033 J. The most difficult projectile to withstand was conical, followed by ogive, hemispherical, and blunt. The results of the core modification on the tetrachiral sandwich structure show that the octagonal core had better energy absorption, by 2.8%, compared to the circular core. Modifying the node geometry in the tetrachiral core and then analyzing it with stress and strain contours are the novel aspects of this research.

Keywords: Sandwich Structures; Tetrachiral Core; Absorbed Energy; Military Armor; High-Velocity Impact.

1. Introduction

Energy absorption refers to the loss of input energy from external loading through plastic deformation or fracture [1]. This concept is fundamental in various fields, including engineering, and it explains how materials respond to external forces, such as pressure or impact. The concept of absorbed energy is widely applied in various fields, including the military field [2]. In the military field, energy absorption analysis is applied to minimize the effects of ballistic impact, namely impact cases involving projectiles and their targets. One common target in the military field is military vehicles, so they require armor that can withstand projectiles. In the case of high-velocity impact, the velocity of a projectile can be more than 50 m/s [3, 4]. One way to minimize high-velocity impact is to use a sandwich structure. This structure consists of two outer layers and a core layer [5]. The sandwich structure has the advantage of being lightweight, making it suitable for military tactical vehicles that require fast mobility.

* Corresponding author: aditya@ft.uns.ac.id

http://dx.doi.org/10.28991/CEJ-2024-010-10-017

Many researchers have examined the ballistic impact phenomenon on sandwich structures. Ma et al. [6] investigated the effects of infill patterns on 3D-printed polylactide acid (PLA) sandwich panels under ballistic impact. Infill patterns played an essential role in the 3D-printed sandwich structures in their study. Khalaf and Hamzah [7] conducted experimental and numerical analyses on the structure of hybrid composite sandwich panels under high-velocity impact. In their study, the materials used for the front and back facesheets included ultra-high molecular weight polyethylene, Kevlar, Al_2O_3, and carbon, while the core material used was Al honeycomb. Alam and Aboagye [8] conducted numerical and experimental analyses of segmented sandwich composite armor, including variations in the material, armor height, and armor design configuration. In their research, a ceramic layer, honeycomb core, and composite layer were used to construct the sandwich structure.

Research on sandwich structures continues to be carried out by varying the arrangement of the layers and cores. Sandwich structures using auxetic structural cores have been developed because they increase the energy absorption capability. Sadikbasha & Pandurangan [9] analyzed sandwich structures with auxetic tetrachiral cores under high-velocity impact. They examined the auxetic effect during impact and compared the auxetic cores with hexagonal honeycomb cores. Qin et al. [10] examined axisymmetric tetrachiral honeycombs under in-plane impact. The study examined the energy absorption characteristics and the effect of a negative Poisson's ratio. Atill Yolcu & Okutan Baba [11] investigated the impact behavior of curved sandwich composites with chiral auxetic cores. The study evaluated and compared the energy absorption capabilities of sandwich panels with various chiral auxetic cores. Pham and Huang [12] researched hierarchical tetrachiral structures. They modified the tetrachiral structure by adding new structures to the tetrachiral nodes, and then the structures before and after modification were compared.

The main objective of this research was to analyze a tetrachiral structure with a circular node modified into polygonal shapes, namely square, hexagonal, and octagonal. This has not been carried out in previous studies. The sandwich structure materials used were Armox 500T, AISI 52100, Ti6Al4V, and Al 1100. In addition, the effect of projectile geometry was investigated using ogive, conical, blunt, and hemispherical projectiles. This study employed numerical analysis using ABAQUS software. The numerical analysis methodology was validated through a benchmarking study by comparing the residual velocity results of projectiles with those of previous studies. The results of the numerical analysis include the energy absorption, projectile residual velocity, stress contours, and strain contours.

This paper contains an introduction, which includes the background of the research, a literature review, and the research objectives. Section 2 presents the research flow and validation of the simulation methodology by comparing the results with those of previous studies. In Section 3, the geometry model and mesh convergence are displayed to show the part geometry used in this research; a mesh convergence study was carried out to determine an efficient mesh size. Then, Section 4 discusses the material model and displays the materials used in this study. After that, Section 5 defines the boundary conditions in the impact simulation and discusses the applied simulation model. Next, Section 6 contains the results of the data analysis and a discussion on material variations, projectile geometry, and core geometry. At the end of the paper, conclusions are given to highlight the points of the research that has been carried out.

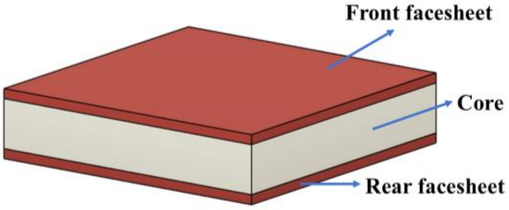

Figure 1. Sandwich structure

2. Research Methodology

This research was carried out in several stages, as shown in Figure 2. In the initial stage, the researchers conducted a review of the literature related to this study. Next, the numerical methods used in the numerical analysis by Sadikbasha & Pandurangan [9] were validated. At this stage, a computational model up to the boundary condition was built from the previous numerical analysis. After that, the results were validated with the numerical results of previous studies. If the error of the analysis results was less than 10%, then we could proceed with the parametric study. In this study, we used Al 1100, Armox 500T, Ti6Al4V, and AISI 52100 materials. Then, the projectile geometry was modified into blunt, ogive, hemispherical, and conical shapes. After that, the core circular geometry was changed to square, hexagonal, and octagonal.

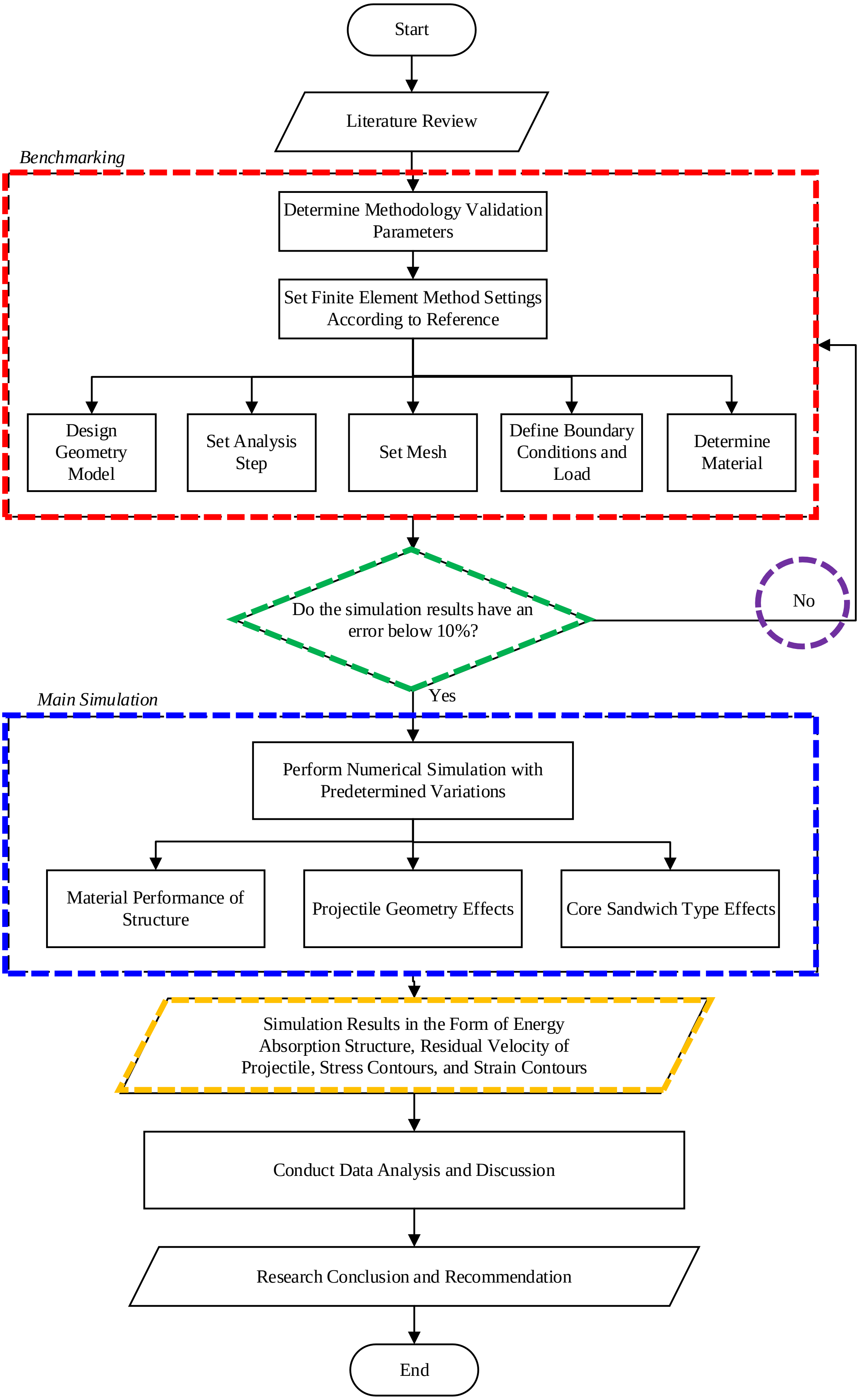

Figure 2. Research methodology

2.1. Benchmark Profile

This research used the same method as that in the study by Sadikbasha & Pandurangan [9]. They examined the energy absorption of sandwich structures with different cores using finite element (FE) models, comparing the FE models with analytical ones to estimate the residual velocity, examine the influence of geometry and velocity on ballistic performance, and calculate the damage inflicted on the structure. As a form of validation, the researchers of this study compared the projectile residual velocity results of the current numerical analysis with those of the numerical analysis in the previous research. In addition, a comparison of the contours of the deformation behavior, material flow, and failure at the target is also displayed.

The numerical analysis in this study was carried out using ABAQUS software. The results were validated using the same parameters and analysis settings as in the previous study by Sadikbasha & Pandurangan [9]. The boundary conditions in the simulation were adjusted to those shown in the experimental scheme in Figure 3. All the degrees of freedom (DOF) at the edges of the face sheet were considered to be zero. The geometries used for this numerical analysis were a blunt projectile and a tetrachiral core. The blunt projectile had a length and diameter of 50.8 and 19 mm, respectively, and a weight of 52.5 g. The material used was Al 1100. The mesh size used was 0.25 mm at the impact region.

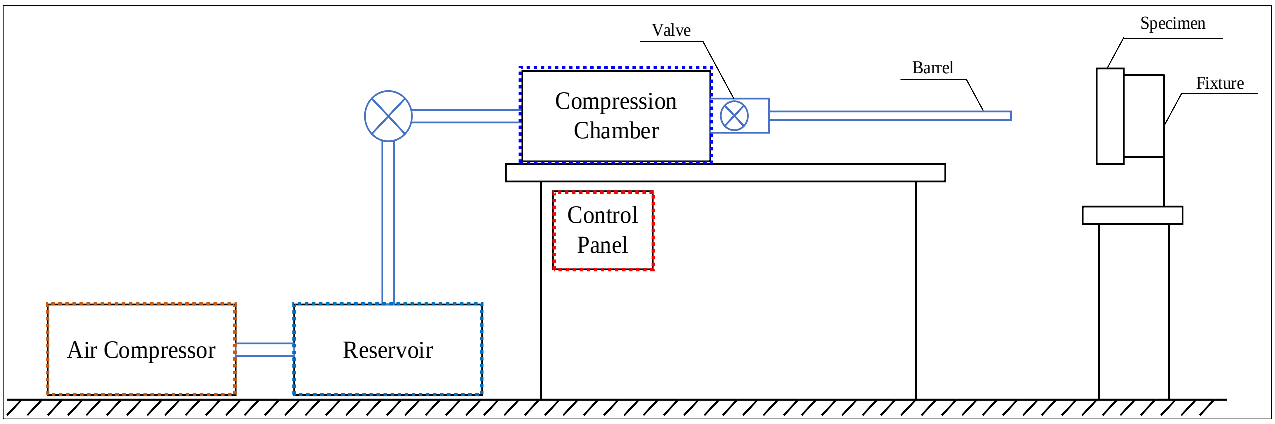

Figure 3. Experimental analysis scheme created by Sadikbasha & Pandurangan [9]

2.2. Benchmarking Results

This simulation used initial projectile velocities of 450, 350, and 250 m/s. Table 1 shows the simulation results of the residual velocity. This simulation used blunt and tetrachiral core projectiles. It can be seen that the projectiles' residual velocities were not too different.

Table 1. Comparison of residual velocity results

Initial velocity (m/s)	Residual velocity (m/s)			Numerical result error (%)
	Analytical result [9]	Numerical result [9]	Numerical result (present study)	
450	381.8	380.4	381.091	0.18
350	278.3	273.8	276.832	1.11
250	161.8	147.9	155.6	5.21

The deformation behavior of the sandwich structure at different times is shown in Figure 4. This figure compares the sandwich structure's deformation at a velocity of 175 m/s from the previous and present studies. At 0.01 ms, the projectile struck the front facesheet. At 0.03 ms, the projectile hit the front facesheet with significant force, which put pressure on the core led to buckling of the ligament and damage to the tetrachiral structure. At 0.09 ms, as shown in previous studies, the projectile penetrated the front facesheet and left a mark with the diameter of the projectile. At 0.18 ms, the projectile bounced after hitting the rear facesheet at a low velocity. Its direction deviated from its original path due to the friction force between the projectile and the core, and the deviation angle was no more than 30°.

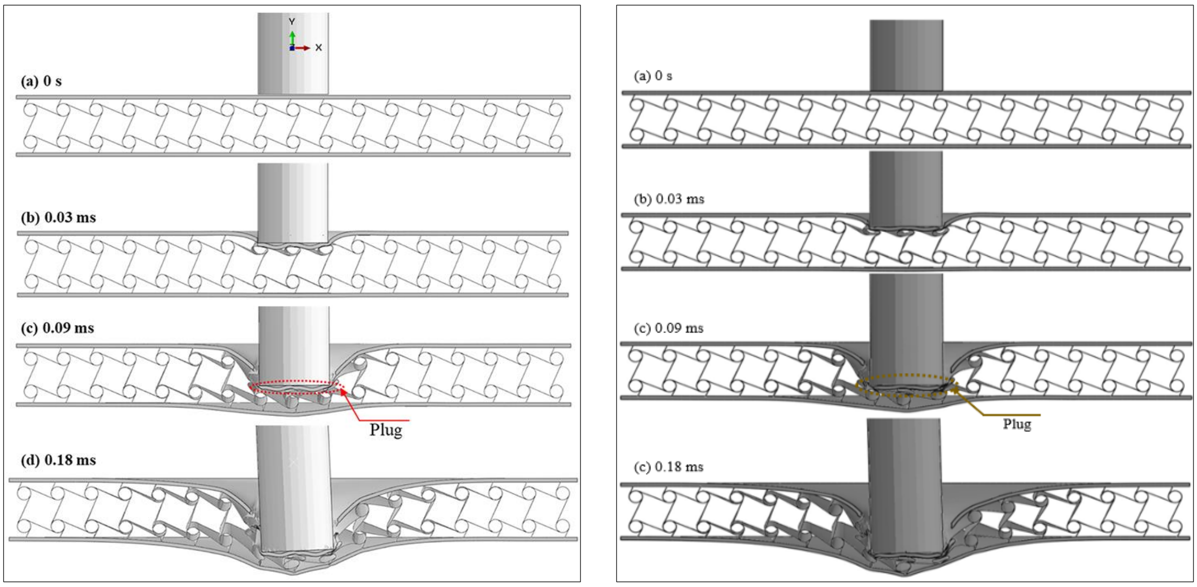

Sadikbasha and Pandurangan [9] Present study

Figure 4. Comparison of deformation modes observed with blunt projectile at 175 m/s in the previous and present study: (a) before impact; (b) core buckling; (c) front facesheet perforation and core crushing; (d) core crushing and rear facesheet buckling [9].

The material flow in this structure is a primary concern because it is auxetic with a negative Poisson ratio. When the material flow leads to the impact area, the impact resistance of the structure is increased. Figure 5 represents a displacement comparison of each section in the z direction at 0.325 ms between the previous and present studies. In the previous study, the average displacement values in the 7th unit cell at Z = 30, 50, and 75 were 0.09, 0.05, and 0.27, and for the 11th unit cell, they were -0.13, -0.17, and -0.20 mm, respectively. In unit cells 2 and 16 at Z = 30 mm, the values were 0.2 and 0.14 mm. The average displacement values in the present study in the 7th unit cell at Z = 30, 50, and 75 were 0.035, 0.16, and 0.39 mm, and the values in the 11th unit cell were -0.31, -0.15, and -0.09 mm, respectively. Furthermore, at Z = 30 mm, the average displacement values in unit cells 2 and 16 were 0.14 and 0.19 mm. The auxetic response of the structure in the previous and present studies can be seen, where the auxetic effect moves away from the impact area.

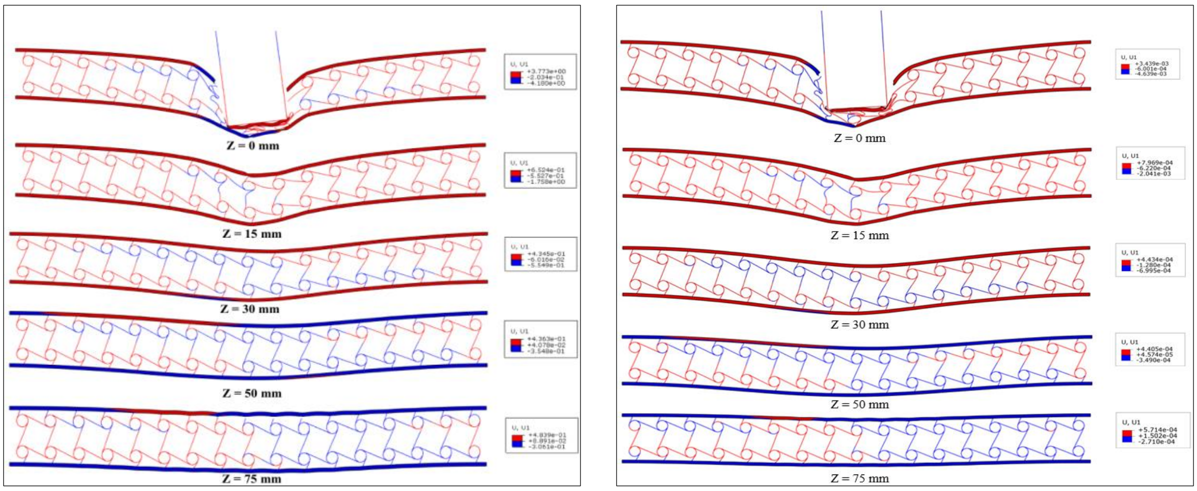

Sadikbasha & Pandurangan [9] Present study

Figure 5. Comparison of displacement contours in a sandwich structure subject to blunt projectile impact at 175 m/s between the previous and present studies [9]

Figure 6 shows failure of the sandwich structure using a blunt projectile at a velocity of 350 m/s. With blunt projectiles, both the front and rear facesheets failed due to shear stress, which caused thinning of the facesheet thickness, leading to fracture. The blunt projectiles left marks that could be seen in the front and back facesheets. The failures in the present study were similar to those in the previous study. The benchmarking results show that the velocities and contours were similar and did not show a significant difference. Thus, the benchmarking methodology can be used for further research.

Study	Projectile	Front facesheet	Sandwich	Rear facesheet	Failure type
Present study	Blunt	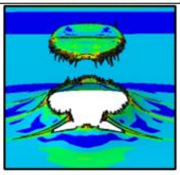	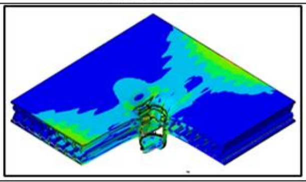	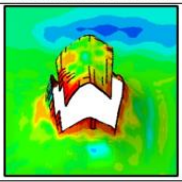	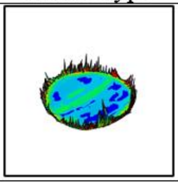
S. Shaik & V. Pandurangan, 2023	Blunt	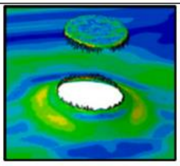	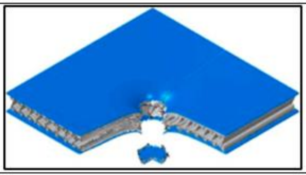	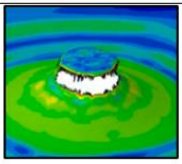	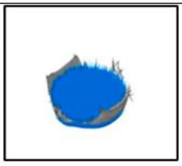

Figure 6. Comparison of failure modes in geometry of sandwich panel at 350 m/s in previous and present studies [9]

3. Geometry Model and Mesh Convergence

3.1. Geometry Model Parametric Study

The simulation in this study involved two parts: the projectile and the sandwich panel. Four projectiles were used: blunt, ogive, hemispherical, and conical (Figure 7). The geometries of the projectiles were the same as those used in the research by Mohammad et al. [13]. All projectiles had the same weight of 52.5 g. In this simulation, the projectile was defined as a discrete rigid. The sandwich panel geometry had three parts: the front facesheet, the core, and the rear facesheet. The facesheet was defined as a deformable solid, and the core was defined as a deformable shell (Figure 8). In this research, we used different core variations, but the geometry was still the same as the tetrachiral geometry in the previous research by Sadikbasha and Pandurangan [9]. The tetrachiral geometry had four circular nodes, which changed into square, hexagonal, and octagonal shapes (Figure 9). Thus, a total of four core geometries was used. The facesheet was 1 mm thick, with an edge length of 150 mm. Furthermore, the core had a height (h) of 15 mm and a unit distance between the unit cells (l) of 8.89 mm, and the radius of the circle vertices (r) had an l/r ratio of 5, so the radius of the circle vertices was 1.778 mm [14]. The interaction between the projectile and the front facesheet was surface-to-surface. The facesheet and the core had tie interaction. General-contact interactions were also added to define the interactions that occurred in all parts.

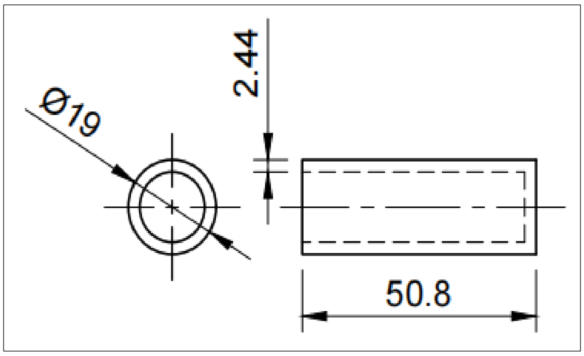

(a)

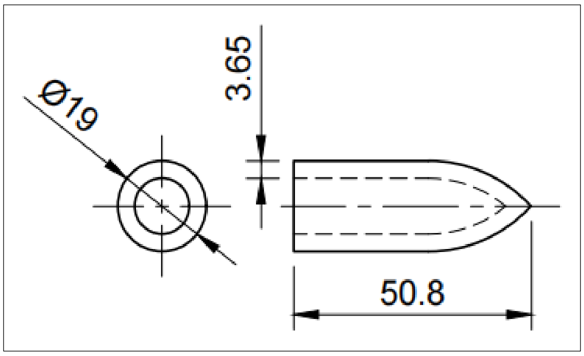

(b)

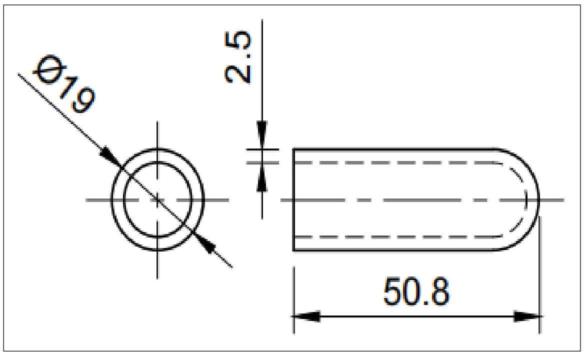

(c)

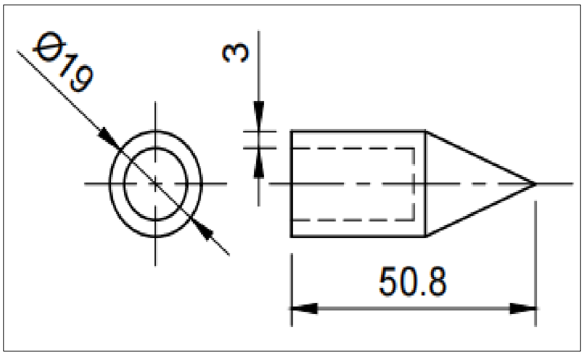

(d)

Figure 7. Geometries of the deployed projectiles: (a) blunt, (b) ogive, (c) hemispherical, and (d) conical [13]

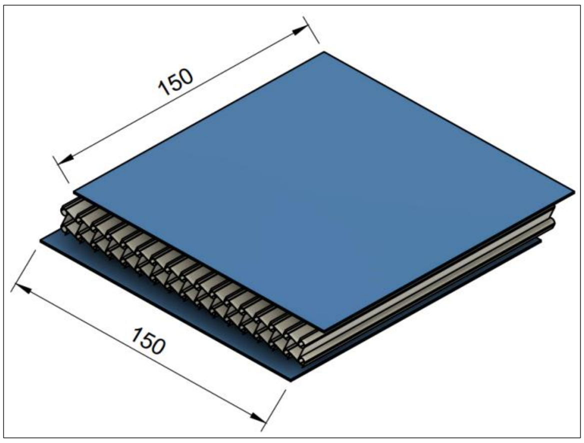

Figure 8. Designed sandwich structure [9]

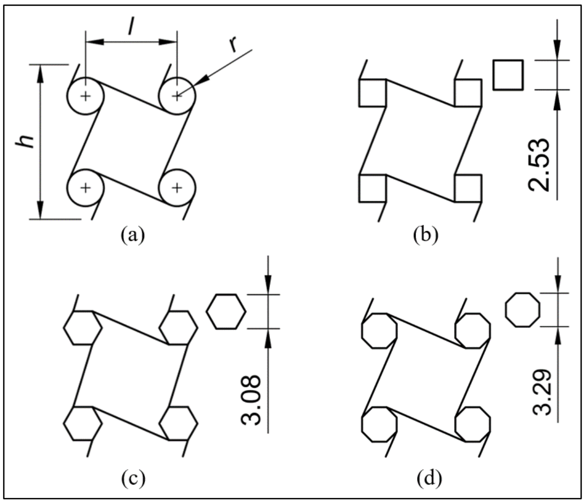

Figure 9. Geometries of (a) circle, (b) square, (c) hexagon, and (d) octagon cores

3.2. Mesh Convergence

Before the parametric study, the efficient mesh size was determined using mesh convergence. Mesh convergence was performed by comparing the mesh size with the residual velocity. As shown in Figure 10, the projectile velocity after hitting the target at mesh sizes of 3 to 16 mm is the rebound velocity. The convergence line can be seen in Figure 10, and the convergent value starts at a mesh size of 3 mm. By adjusting the facesheet mesh, the cores and projectiles were discretized using eight solid nodes (C3D8R), four shell nodes (S4R), and four rigid element nodes (R3D4). The thickness of the facesheet was given a mesh size of 0.25 mm so that the failure results could be seen accurately. Therefore, a mesh size of 3 mm was used for this study to make the simulation more effective. In Figure 11, computational models for finite element simulation are shown.

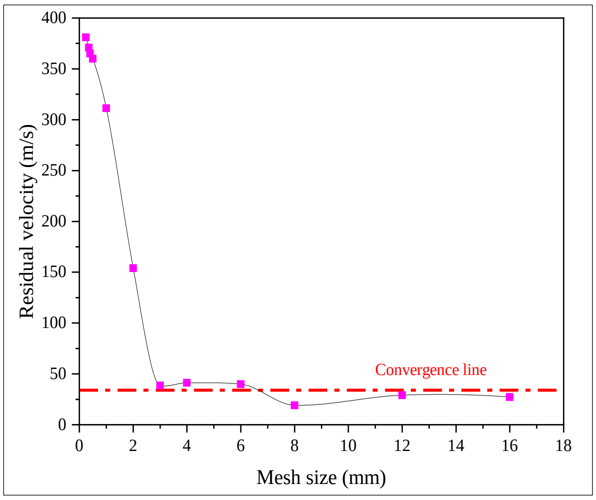

Figure 10. Mesh convergence results

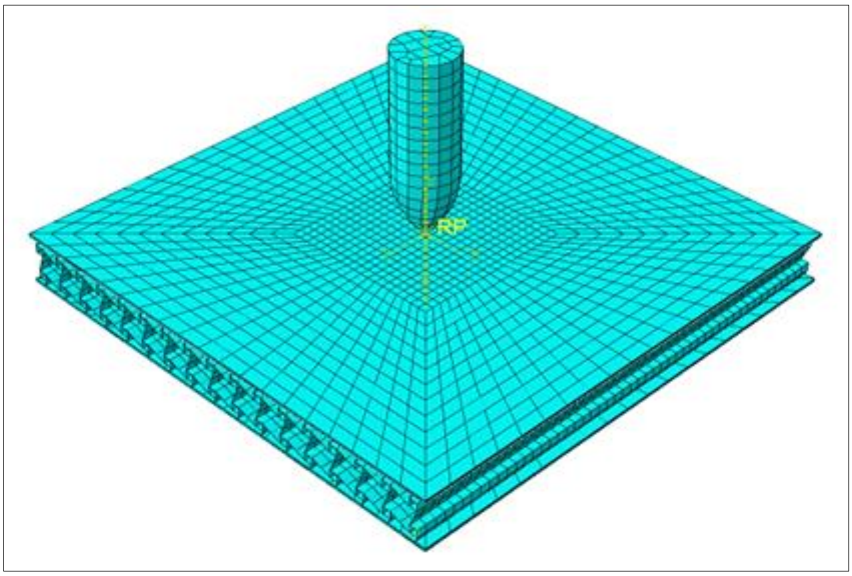

Figure 11. Computational model for finite element simulation

4. Material Properties

High-velocity impact analysis is a dynamic analysis, meaning that it takes into account changes in time. The deformation that occurred in this analysis was very fast, in contrast to static analysis, where deformation occurs slowly. The combined effects of strain, strain rate, and temperature were considered. Therefore, the Johnson–Cook (JC) material model was used. The materials used in this research were Al 1100, Armox 500T, Ti6Al4V, and AISI 52100. These materials are used in automotive components [15–17]; specifically, Armox 500T is used for military vehicle armor [18, 19]. The facesheet and core undergo significant plastic deformation, strain hardening, and thermal softening upon impact. The Johnson–Cook material model was used to explain the strain rate response of the target material. Deformations in the projectile were ignored and considered a rigid object. In the JC model, the equivalent stress ($\bar{\sigma}$) can be expressed as presented in Equation 1 [20].

$$\bar{\sigma} = [A + B(\bar{\varepsilon}^{pl})^n]\left[1 + C ln\left(\frac{\dot{\bar{\varepsilon}}^{pl}}{\dot{\bar{\varepsilon}}_0}\right)\right][1 - \hat{T}^{\,m}] \tag{1}$$

A, *B*, *n*, *C*, and m are material parameters obtained from several tests. $\dot{\bar{\varepsilon}}_0$ adalah is reference strain rate, $\bar{\varepsilon}^{pl}$ is equivalent plastic strain, $\dot{\bar{\varepsilon}}^{pl}$ is equivalent plastic strain rate, and $\hat{T}$ a unit less parameter related to temperature and defined as Equation 2.

$$\hat{T} = \frac{T_c - T_t}{T_{melt} - T_t} \text{ for } T_t < T_c < T_m \tag{2}$$

where $T_c, T_t,$ and T_{melt} are instaneous, transition, and melting temperature. Then, the Johnson-Cook fracture model requires strain rate, the influence of stress triaxiality, and temperature on the equivalent failure strain. The equivalent fracture strain in the Johnson-Cook model is expressed as Equation 3.

$$\bar{\varepsilon}^{pl} = \left[D_1 + D_2 \exp\left(D_3 \frac{\sigma_m}{\bar{\sigma}}\right)\right]\left[1 + D_4 \ln\left(\frac{\dot{\bar{\varepsilon}}^{pl}}{\dot{\varepsilon}_0}\right)\right][1 + D_5\,\hat{T}] \tag{3}$$

where D_1 until D_5 are material parameters obtained from different mechanical tests, D_1, D_2, and D_3 are stress triaxiality parameters, D_4 is strain rate-dependent damage parameters, D_5 is temperature-dependent fracture strain parameters, $\frac{\sigma_m}{\bar{\sigma}}$ is stress ratio triaxiality, σ_m is average stress, and $\bar{\sigma}$ is equivalent stress.

In ABAQUS software, the material was input by determining the material properties, as shown in Table 2. This study used the Johnson–Cook material model, so the JC parameters define the plasticity and material damage. The plasticity of the material was modeled by entering the values of *A*, *B*, *n*, *m*, melting temperature, and transition temperature then the rate dependent value of *C* and $\dot{\varepsilon}_0$ is entered. Then, the values of D_1, D_2, D_3, D_4, melting temperature, and transition temperature were used to define the damage to the material. After the material properties were determined, material sections were created, using solid–homogeneous for the facesheet and shell–homogeneous for the core. After that, the sections that were created were assigned to the geometry.

Table 2. Material properties [9, 18, 21, 22]

	Unit	Al 1100	Armox 500T	Ti6Al4V	AISI 52100
Density (ρ)	Kg/m^3	2700	7850	4430	7810
Modulus of elasticity (E)	MPa	65762	201000	113000	200000
Poisson's ratio		0.3	0.33	0.33	0.3
Initial yield stress (A)	MPa	148.361	1372.488	1098	774.48
Hardening coefficient (B)	MPa	345.513	835.022	1092	134
Hardening exponent (n)		0.183	0.24670	0.93	0.3700
Strain rate constant (C)		0.001	0.06170	0.014	0.0180
Thermal softening constant (m)		0.859	0.84000	1.1	3.1710
Reference strain rate ($\dot{\varepsilon}_0$)	s^{-1}	1	1	1	0.0001
Melting temperature (T_{melt})	K	893	1800	1878	1424
Transition temperature (T_0)	K	293	293	293	300
Specific heat (C_p)	J/kgK	920	455	580	745
Inelastic heat fraction (η)		0.9	0.9	0.9	0.9
JC damage material constant (D_1)		0.071	0.04289	-0.09	0.0368
JC damage material constant (D_2)		1.248	2.1521	0.27	2.3400
JC damage material constant (D_3)		1.142	-2.7575	0.48	-1.4840
JC damage material constant (D_4)		0.147	-0.0066	0.014	0.0035
JC damage material constant (D_5)		0.000	0.8600	3.87	0.4110

5. Boundary Condition and Simulation Scenario

5.1. Boundary Condition Parametric Study

As shown in Figure 3, in their experimental study, Sadikbasha & Pandurangan [9] used a gas gun set up with a long barrel. Then, the specimen was clamped along all four edges, aligned. Based on the boundary conditions in the experimental test, the boundary conditions in the simulation were adjusted accordingly (Figure 12). All displacement and rotational degrees of freedom (DOF) at the front and rear facesheet edges were constrained (U1=U2=U3=R1=R2=R3=0) because the facesheet was attached to a rigid object. Then, the core was considered to be squeezed by both facesheets and was only given a tie constraint interaction. The projectile was only given a vertical DOF (U2) because, in this study, air resistance was ignored. The initial impact velocity of 450 m/s, which was defined in the translational direction only, was given at the reference point in the projectile by using the predefined field feature.

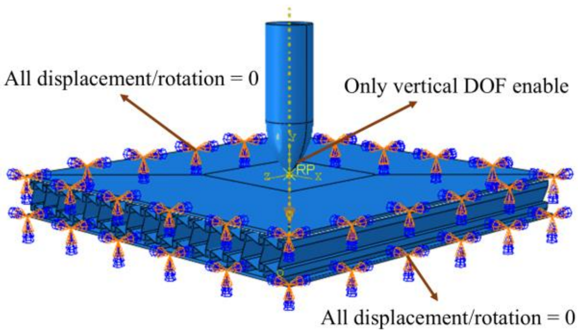

Figure 12. Applied boundary conditions

5.2. Simulation Scenario for Parametric Study

The parameters used in this simulation were the material, core geometry, and projectile type. The materials used were Al 1100, Armox 500T, Ti6Al4V, and AISI 52100. The cores used were a circle, square, hexagon, and octagon. The projectiles used were blunt, hemispherical, conical, and ogive. The projectile velocity for all scenarios was the same, at 450 m/s. A variety of materials and projectiles was used to find materials with high energy absorption. A variety of projectiles was also used to determine the effect of each type of projectile on the target. The core type was also investigated to determine its effect on the sandwich structure. Modeling was performed by designing the projectile, core, and facesheet parts. After all the parts were designed, assembly is carried out on the parts according to the model. After that, the geometry was applied to the material according to the model. Subsequently, we set the interval in ABAQUS

[23-30] using the dynamic explicit procedure [31-35] and set the time period to 0.0008 s. The dynamic explicit procedure was used because, in the case of ballistic impact, the loading time is very short, and this procedure can handle dynamic changes well. In the case of impact, there was also a significant deformation, and the interaction between the material surfaces was dynamic. After setting up the procedure, the simulation output was set to the values of energy, projectile residual velocity, stress, and strain [36-39].

Table 3. Simulation scenarios

Model	Material	Core Geometry	Projectile
1	Al 1100	Square	Ogive
2	Armox 500T	Square	Ogive
3	Ti6Al4V	Square	Ogive
4	AISI 52100	Square	Ogive
5	Armox 500T	Octagon	Blunt
6	Armox 500T	Octagon	Ogive
7	Armox 500T	Octagon	Hemispherical
8	Armox 500T	Octagon	Conical
9	Al 1100	Circle	Hemispherical
10	Al 1100	Square	Hemispherical
11	Al 1100	Hexagon	Hemispherical
12	Al 1100	Octagon	Hemispherical

6. Parametric Study Results

The numerical analysis results in this research were the residual velocity and energy absorption data. The residual velocity was taken as the initial velocity until the projectile penetrated or bounced. The energy absorption was taken as when the projectile penetrated or the projectile velocity became zero. Additionally, the distributions of the stress and strain contours are also provided. The strain value used was plastic strain.

6.1. Material Performance

The materials used in this simulation were Al 1100, Armox 500T, Ti6Al4V, and AISI 52100. It can be seen in Figure 13 that Armox 500T had the highest performance compared to the other three materials. In Figure 13, at a time of 0.11 ms, Armox 500T absorbed 5033.09 J of energy and decreased the projectile velocity to zero. Furthermore, the absorption energy values of AISI 52100 and Ti6Al4V were 4724.33 and 4627.58 J. Al 1100 was the lowest performing material and could only absorb 2644.69 J of energy. Furthermore, Ti6Al4V and AISI 52100 had similar results despite having relatively different densities.

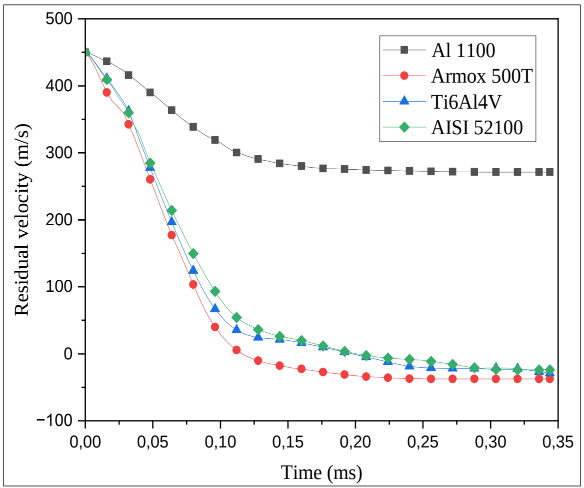

(a)

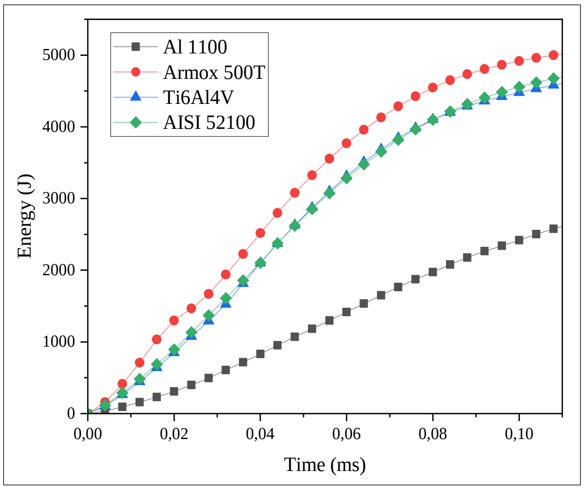

(b)

Figure 13. Graphs of (a) residual velocity and (b) energy absorption of sandwich structure with material variations (models 1, 2, 3, and 4)

The absorption energy value of Armox 500T was the highest because it has a high hardness of about 500 HBW (Brinell Hardness), so it can withstand plastic deformation. In addition, this material has high toughness properties. The toughness value of the material itself can be taken from the stress–strain graph of the tensile test, which was calculated as the area under the curve. Materials with high stress values do not necessarily have high toughness properties, and materials with high strain values do not. Materials that have good toughness have a balance in their stress and strain values. Ti6Al4V was the material with the second-best energy absorption capability after Armox 500T. Although its energy absorption value was below that of Armox 500T, Ti6Al4V had a smaller density, so the weight of the sandwich structure with Ti6Al4V material was lighter than that with Armox 500T by 43%. The advantage of Ti6Al4V, which has a perfect ratio of strength to weight, is that it is very suitable for use in military tactical vehicles with high mobility. Ti6Al4V or titanium grade 5 has a high absorption ability due to its toughness. It can be seen in the material table that the elastic modulus value of Ti6Al4V is between those of steel and aluminum, meaning that this material has a high toughness value because its stress–strain curve is balanced.

The stress value, (as presented in Figure 14) on the Armox 500T structure was 3764 MPa at 0.64 ms, is the highest stress. Furthermore, the stress values on the Ti6Al4V, AISI 52100, and Al 1100 materials were 2690, 1299, and 556.8 MPa, respectively. The high stress value of Armox 500T is due to its very high hardness, meaning that less elastic deformation is experienced. Furthermore, Al 1100 has the smallest stress value because this material has the highest elasticity among all the materials tested. In terms of the strain contour, the value of Al 1100 is found to be 2.727 as shown in Figure 15.

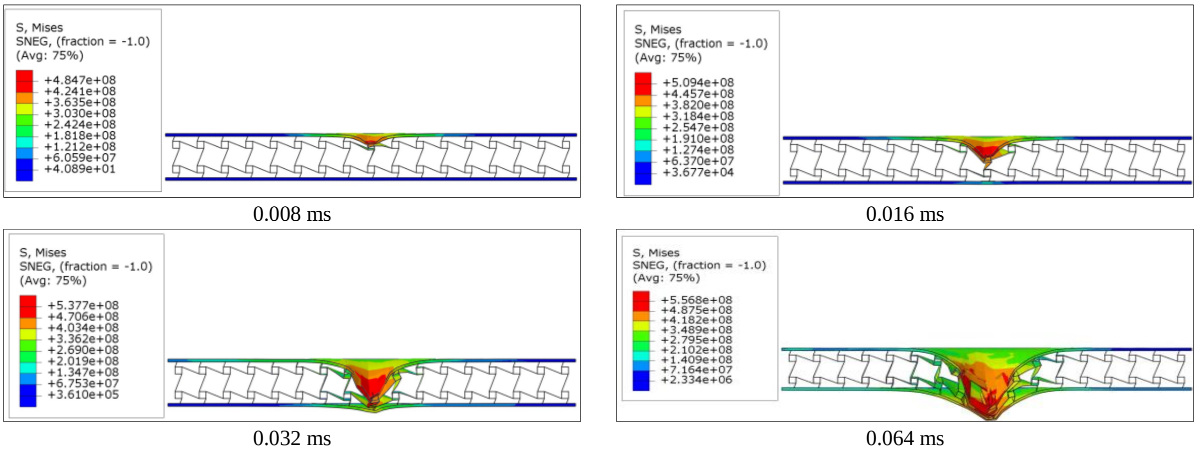

(a) Al 1100 (model 1).

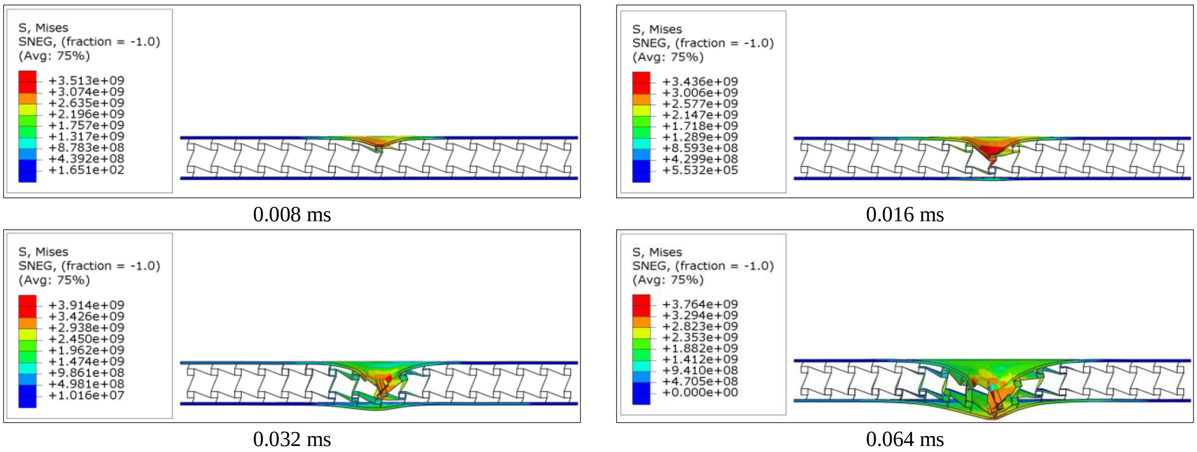

(b) Armox 500T (model 2).

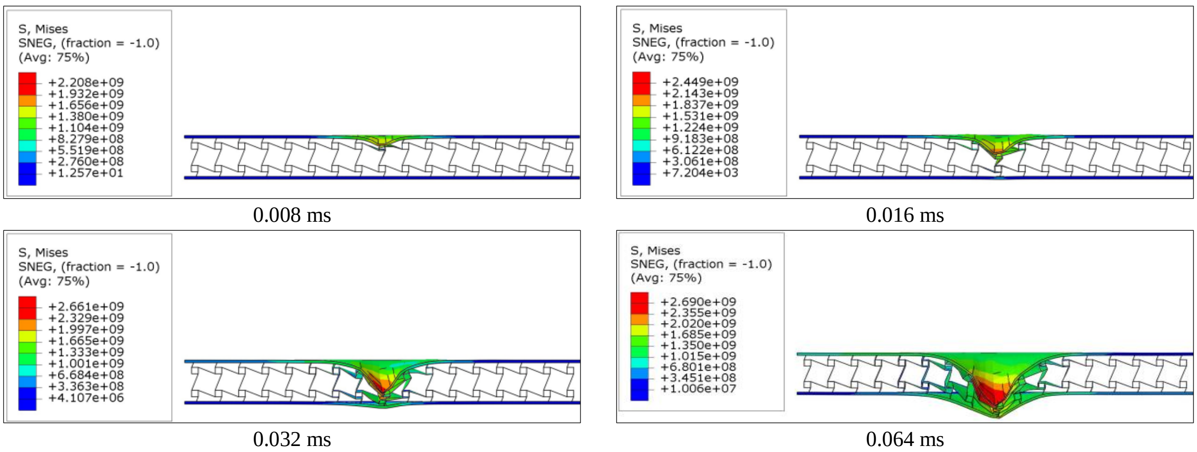

(c) Ti6Al4V (model 3).

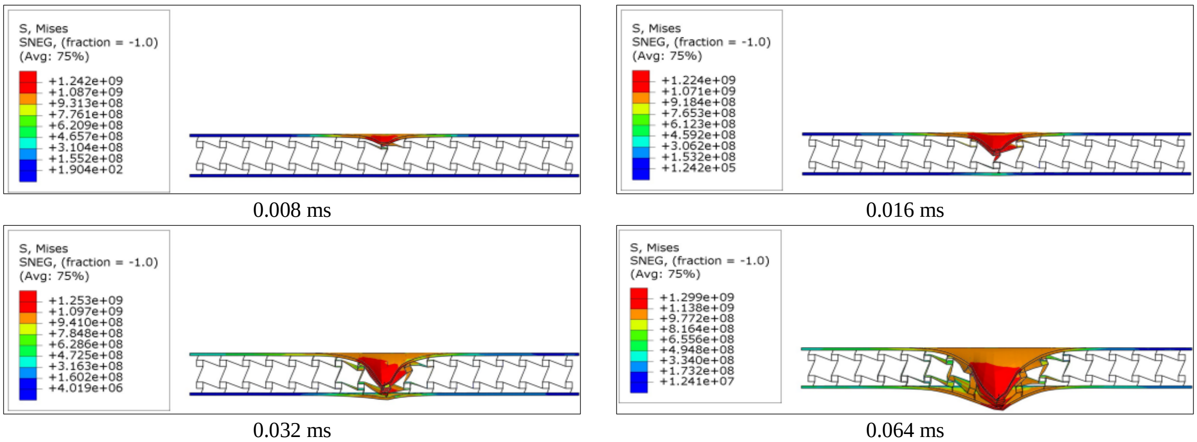

(d) AISI 52100 (model 4).

Figure 14. Stress contours of sandwich structures made with (a) Al 1100, (b) Armox 500T, (c) Ti6Al4V, and (d) AISI 52100 materials

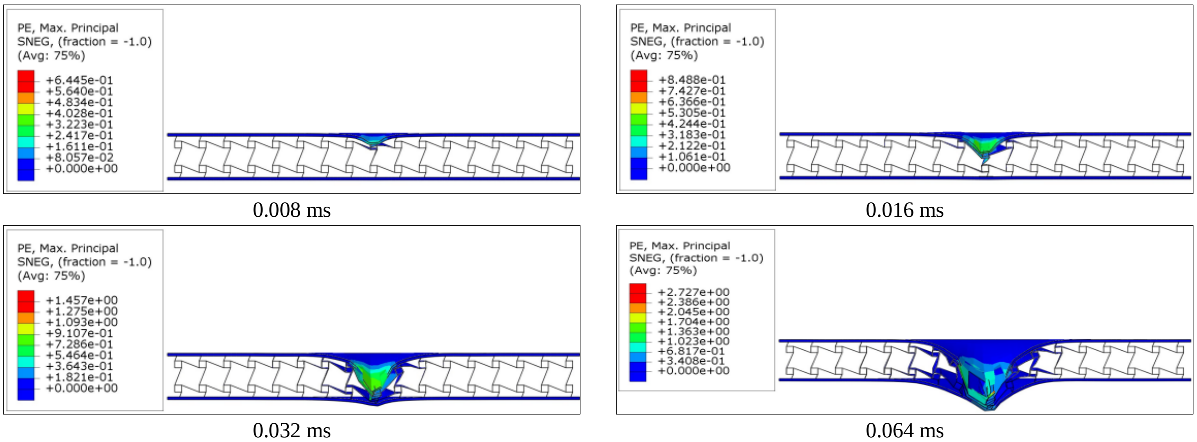

(a) Al 1100 (model 1).

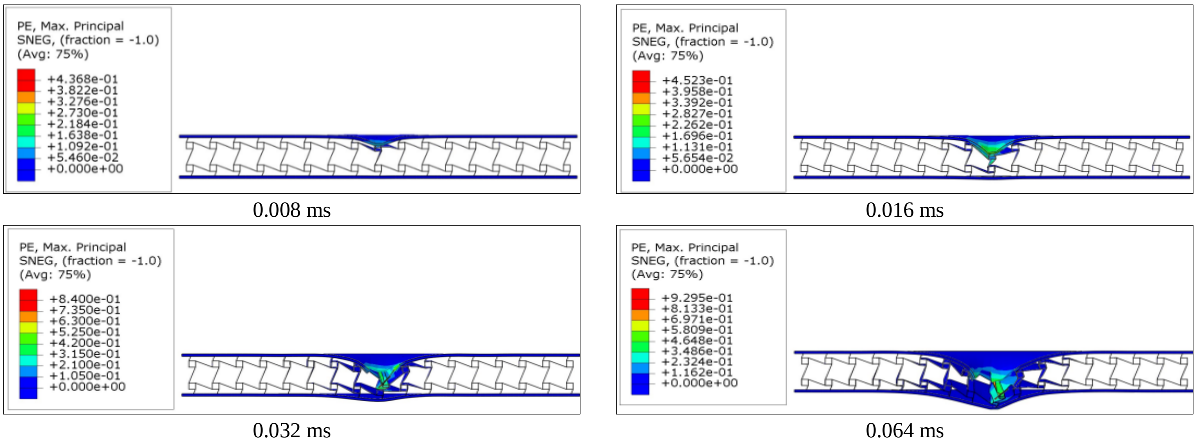

(b) Armox 500T (model 2).

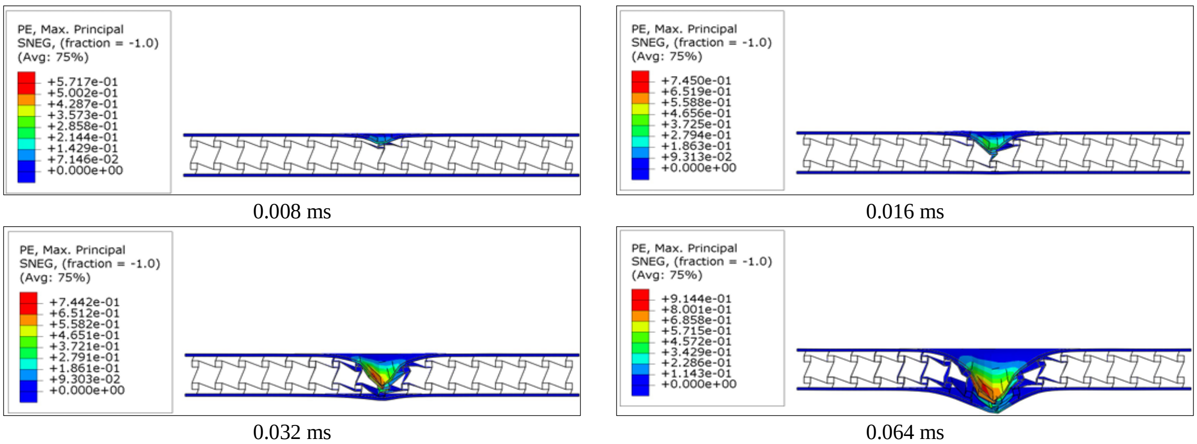

(c) Ti6Al4V (model 3).

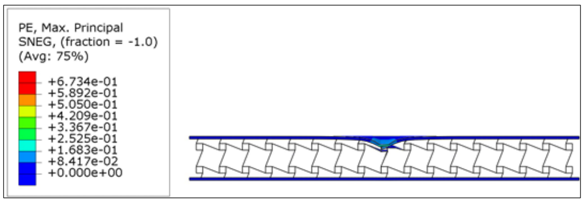

0.008ms

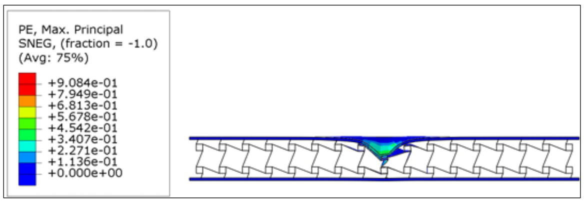

0.016 ms

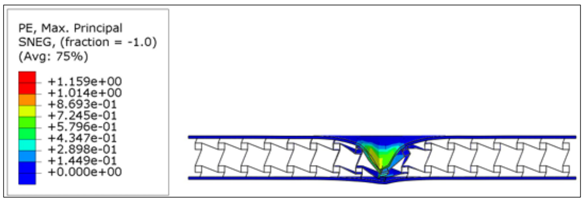

0.032 ms

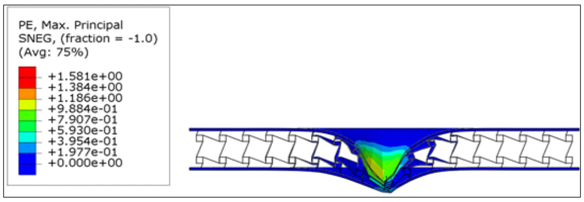

0.064 ms

(d) AISI 52100 (model 4).

Figure 15. Strain contours of sandwich structures made with (a) Al 1100, (b) Armox 500T, (c) Ti6Al4V, and (d) AISI 52100 materials

6.2. Projectile Geometry Effects

For this simulation, four projectile types were used: blunt, ogive, hemispherical, and conical. The materials and cores used were Armox 500T and octagonal. Figure 16 shows that the blunt projectile's velocity was the slowest to decrease, so the target's absorption energy value was high, at 5039 J. This was followed by the hemispherical, ogive, and conical projectiles at 4990, 4966, and 4950 J. According to the target absorption energy values, the geometry of the projectile plays an important role in impact cases because it affects the impact behavior.

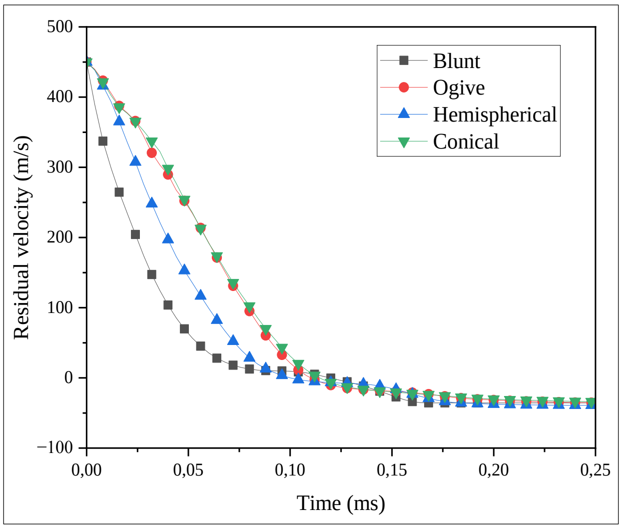

(a)

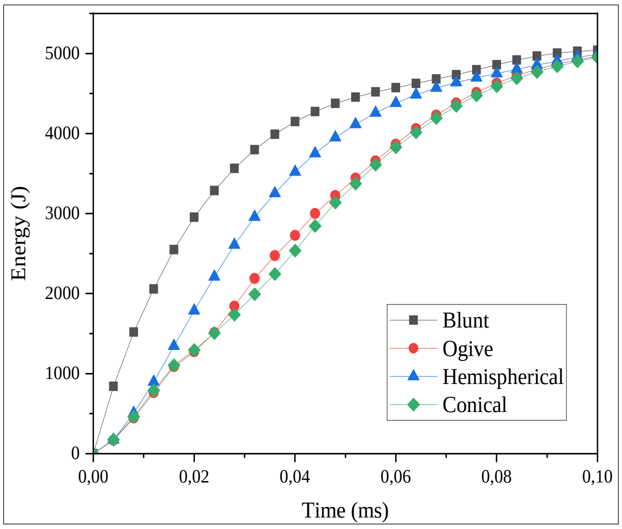

(b)

Figure 16. Graphs of (a) residual velocity and (b) energy absorption of sandwich structures with different projectiles (models 5, 6, 7, and 8).

Figure 17 shows the different stress contours of the four different types of projectiles. At 0.064 ms, the highest stress value was obtained for the conical projectile at 3801 MPa, followed by the ogive at 3540 MPa. These projectiles produce high stress values concentrated in an area, namely the area of the structure exposed to the tip of the projectile. This high stress value is caused by the angle of the pointed projectile. The contact surface area between the projectile and the structure is smaller, making the stress value more significant because the force from the projectile is distributed on a small area. Thus, the area with the high stress concentration experiences failure. It can be seen that at 0.032 ms, the conical and ogive projectiles started to push out the front facesheet.

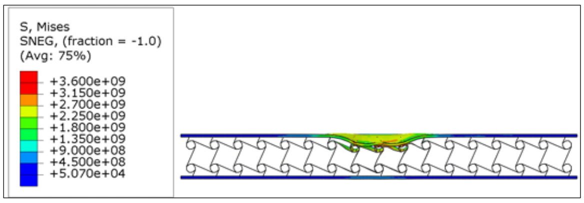

0.008 ms

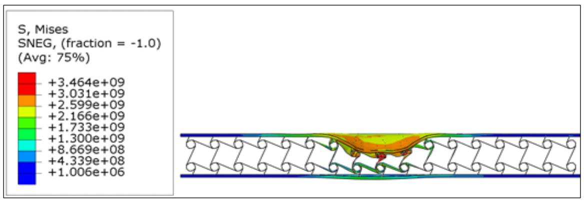

0.016 ms

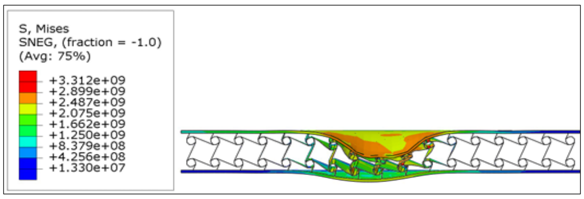

0.032 ms

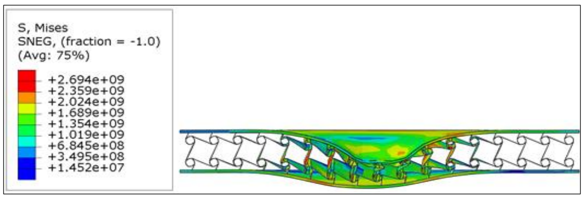

0.064 ms

(a) Blunt (model 5).

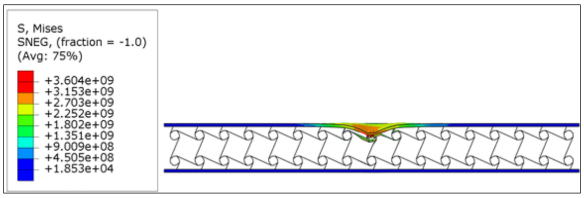

0.008 ms

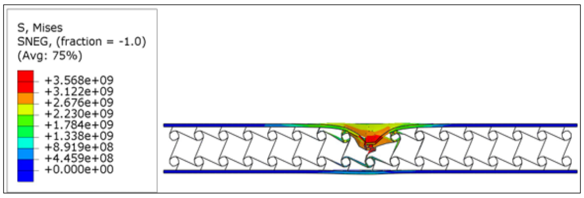

0.016 ms

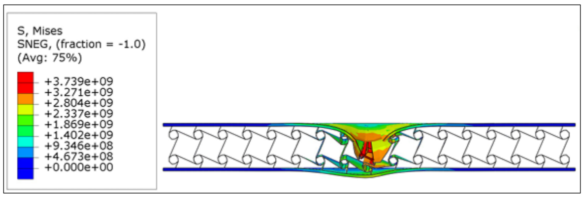

0.032 ms

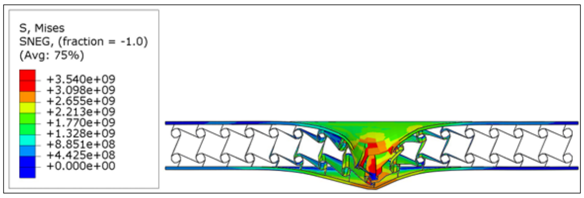

0.064 ms

(b) Ogive (model 6).

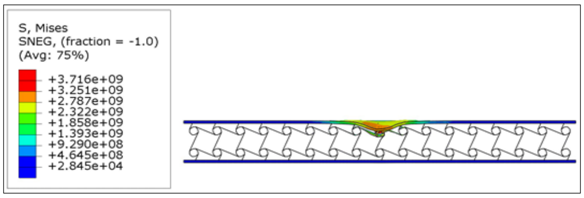

0.008 ms

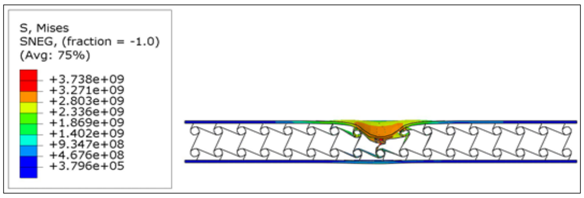

0.016 ms

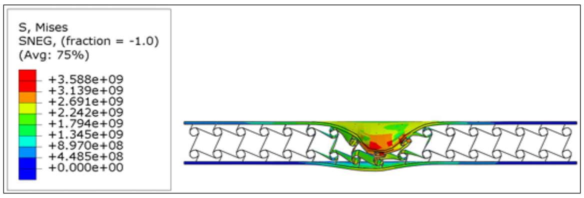

0.032 ms

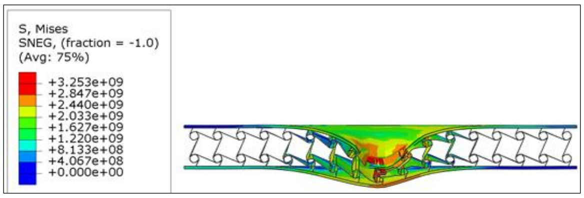

0.064 ms

(c) Hemispherical (model 7)

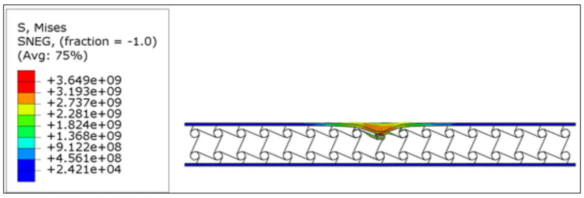

0.008 ms

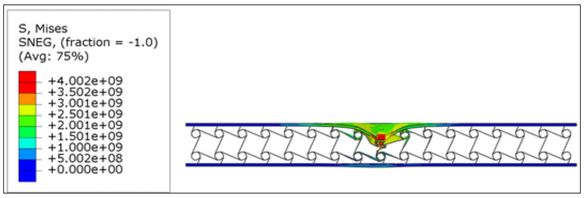

0.016 ms

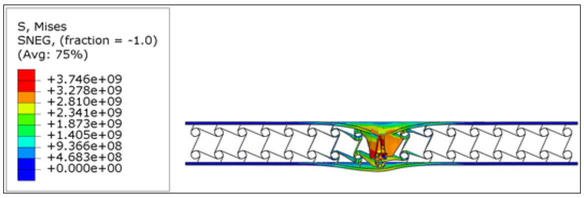

0.032 ms

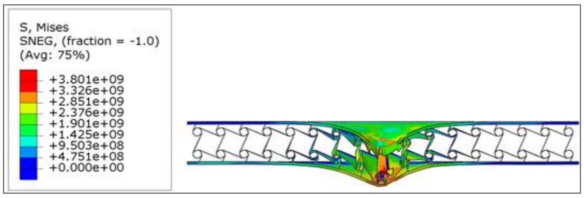

0.064 ms

(d) Conical (model 8).

Figure 17. Stress contours of sandwich structures hit with (a) blunt, (b) ogive, (c) hemispherical, and (d) conical projectiles

A hemispherical projectile has a tip that is shaped like a semicircle. This projectile geometry caused significant and centralized stress at the beginning of impact because the contact surface area was relatively small. However, at 0.032 to 0.064 ms, the surface area in contact with the target became large, so the stress decreased, but the target experienced a sizeable tensile stress on the side of the projectile tip. The front facesheet experienced tensile stress on the side area of the projectile tip until thinning and failure occurred and the projectile began to penetrate the front facesheet. Furthermore, with the blunt projectile, the stress at the tip of the projectile was evenly distributed, but the corner of the projectile tip produced high stress that could be seen at 0.008 ms. This is because the angle at the tip of the corner was sharp, so it produced high stress in that area. This projectile created failure due to the high shear stress value at the corner of the projectile, but it could still not penetrate the front facesheet until 0.064 ms.

It can be seen in Figure 18 that at 0.008 to 0.064 ms, the strain values of the blunt and hemispherical projectiles increase insignificantly, and at 0.032 to 0.064 ms, the stress values tended to stagnate. This is in contrast to the strain characteristics of the ogive and conical projectiles, the increase in which tended to be linear. This shows that the surface area of the projectile can affect the strain characteristics.

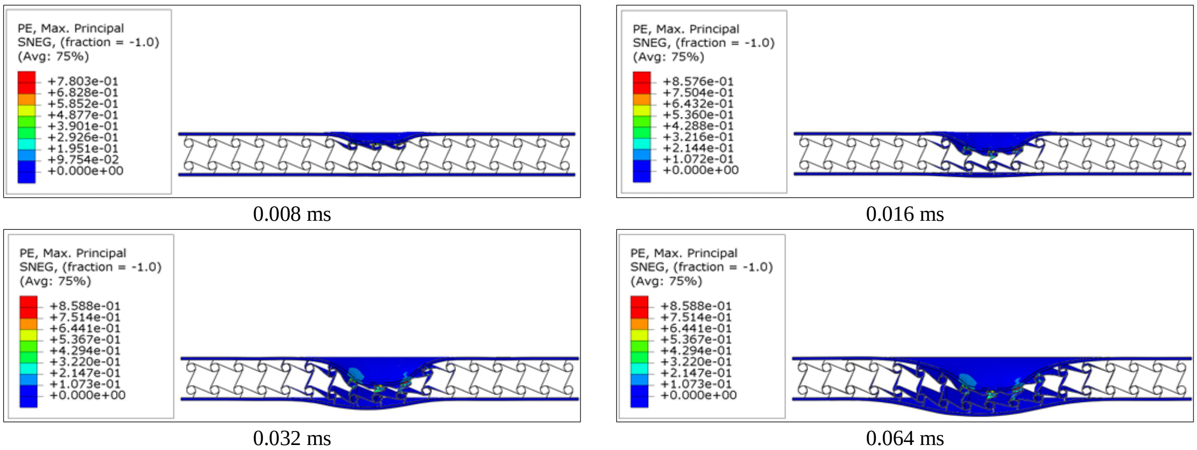

(a) Blunt (model 5).

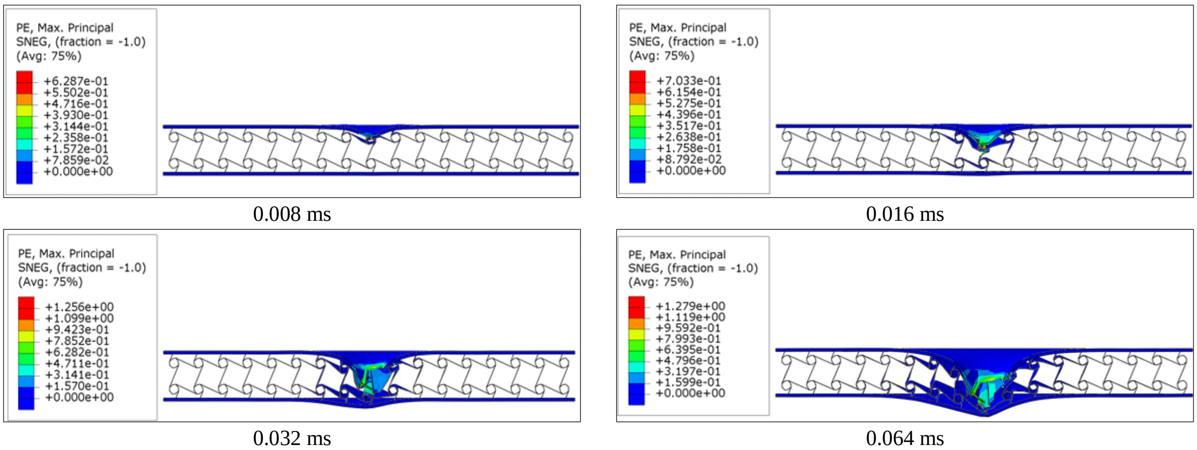

(b) Ogive (model 6).

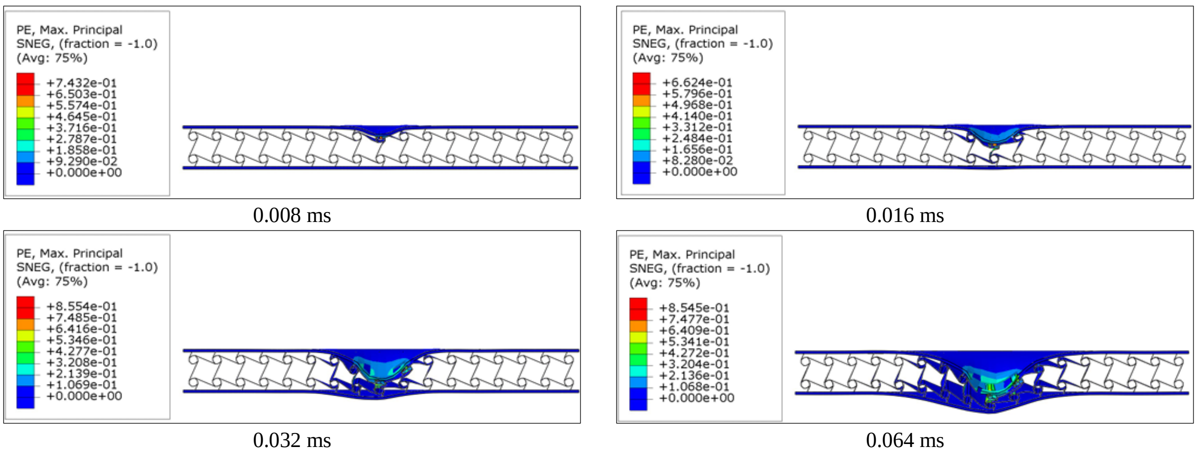

(c) Hemispherical (model 7).

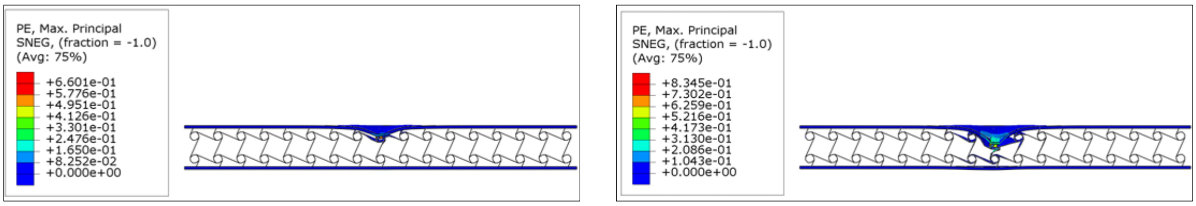

0.008 ms 0.016 ms

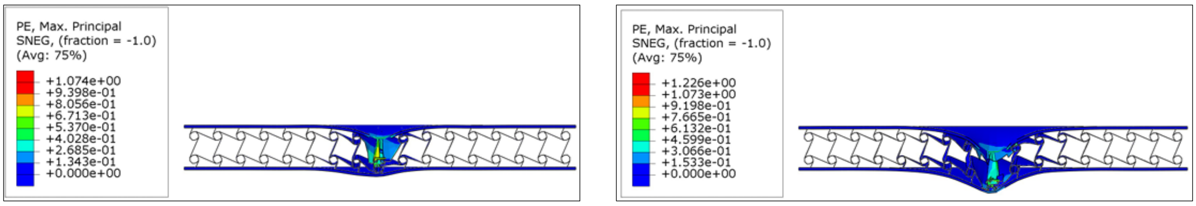

0.032 ms 0.064 ms

(d) Conical (model 8).

Figure 18. Strain contours of sandwich structures hit with (a) blunt, (b) ogive, (c) hemispherical, and (d) conical projectiles

6.3. Core Sandwich Type Effects

In this study, we modified the geometry of tetrachiral sandwich cores with a circular node shape to polygonal geometry: square, hexagon, and octagon. The projectile and material used were hemispherical and Al 1100, respectively. Figure 19 shows that the octagon core performed better. The octagon core resulted in a residual projectile velocity of 209.01 m/s from an initial velocity of 450 m/s. The energy absorbed was also the highest among all of the cores, at 4088.26 J. The values of energy absorbed by the square, circle, and hexagon cores were 4079.63, 3973.28, and 3743.06 J. These data show that modification can increase the absorption energy of the tetrachiral sandwich structure by 2.8%. The octagon geometry improved the performance of the sandwich structure because the plastic region that occurred in this geometry was in the corners, so it was more difficult to deform and more resistant to load.

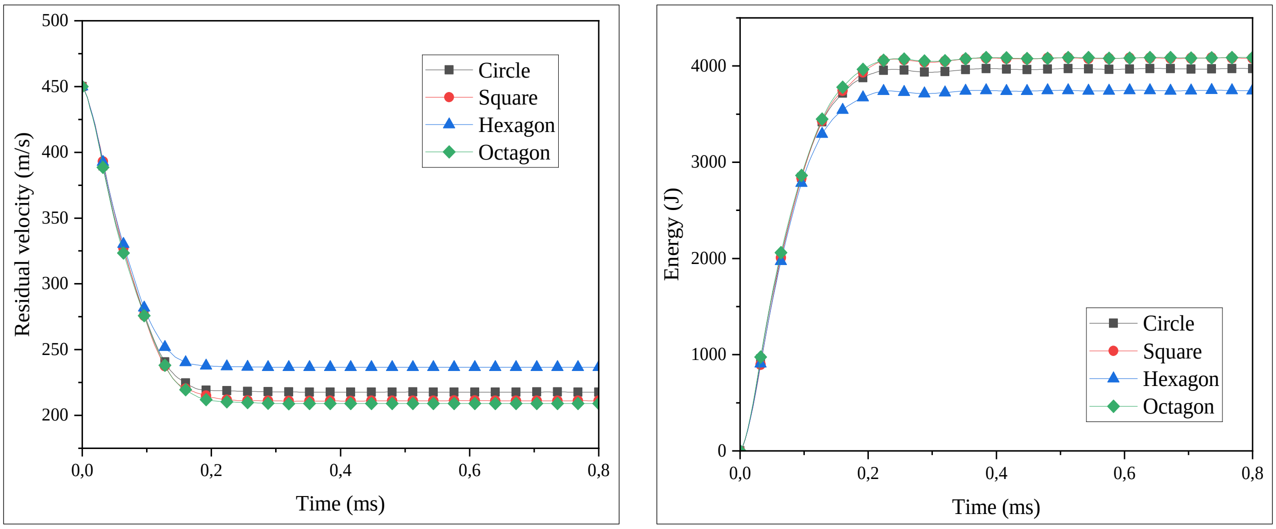

(a) (b)

Figure 19. Graphs of (a) residual velocity and (b) energy absorption of sandwich structures with different cores (Models 9, 10, 11, and 12)

Figures 20 and 21 show the stress and strain of the various cores. The circular core had the highest stress of 571.2 MPa. The stress values of the square, octagonal, and hexagon cores were 557.7, 542.6, and 537.9 MPa, respectively, showing that they did not differ much. The most considerable strain was found with the circular core at 2.638, followed by the octagonal, square, and hexagon cores at 1.7, 1.58, and 1.55. This shows that modifying the core into a polygonal shape can cause the sandwich structure to stiffen. The rear facesheet on the octagon core took longer to penetrate than the circular core, but the timing was not very different.

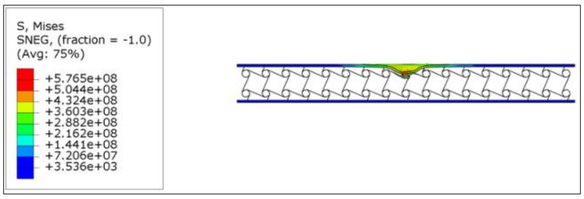

0.008 ms

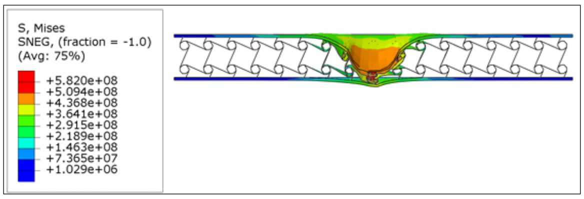

0.032 ms

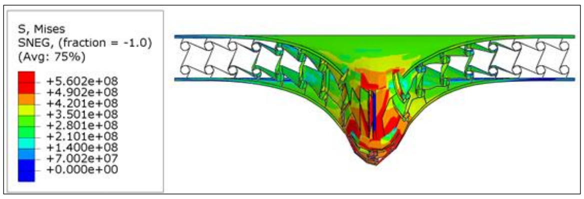

0.128 ms

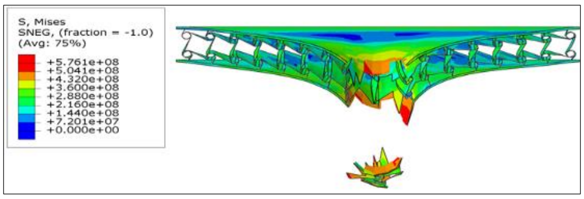

0.256 ms

(a) Circle (model 9).

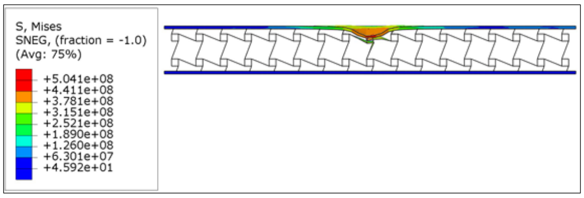

0.008 ms

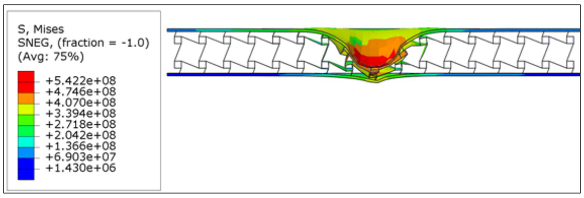

0.032 ms

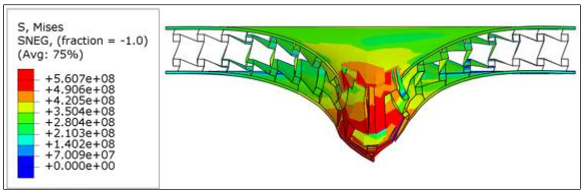

0.128 ms

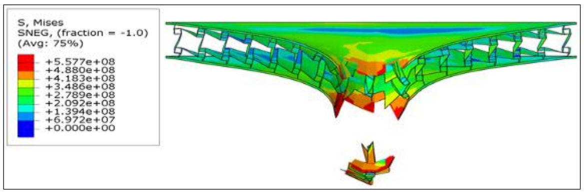

0.256 ms

(b) Square (model 10).

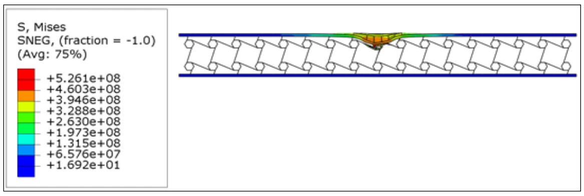

0.008 ms

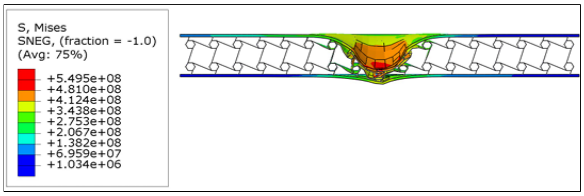

0.032 ms

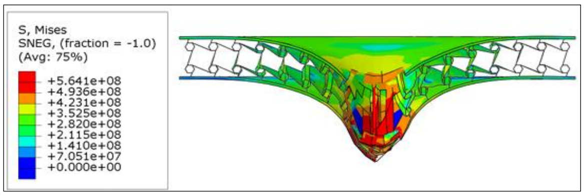

0.128 ms

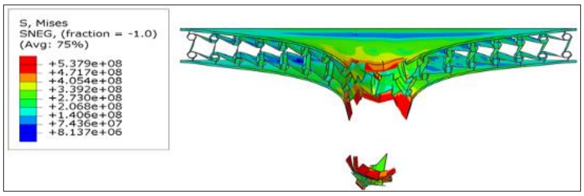

0.256 ms

(c) Hexagon (model 11).

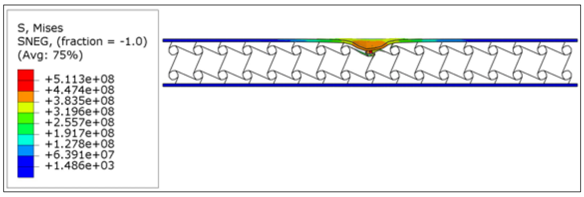

0.008 ms

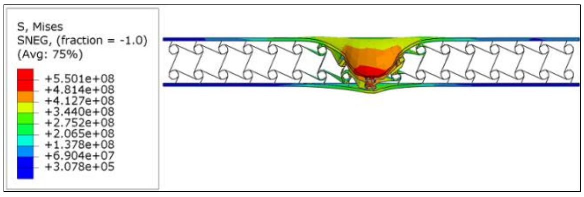

0.032 ms

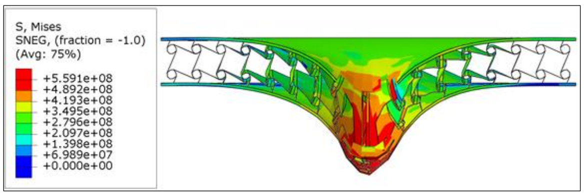

0.128 ms

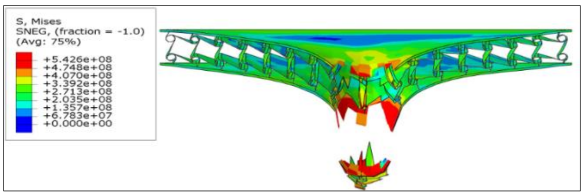

0.256 ms

(d) Octagon (model 12).

Figure 20. Stress contours of sandwich structures with (a) circle, (b) square, (c) hexagon, and (d) octagon cores

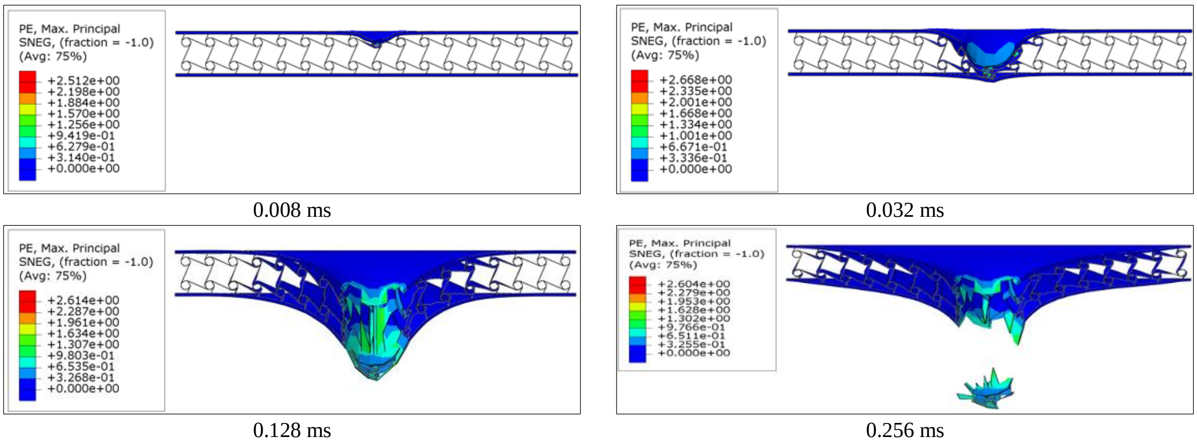

(a) Circle (model 9).

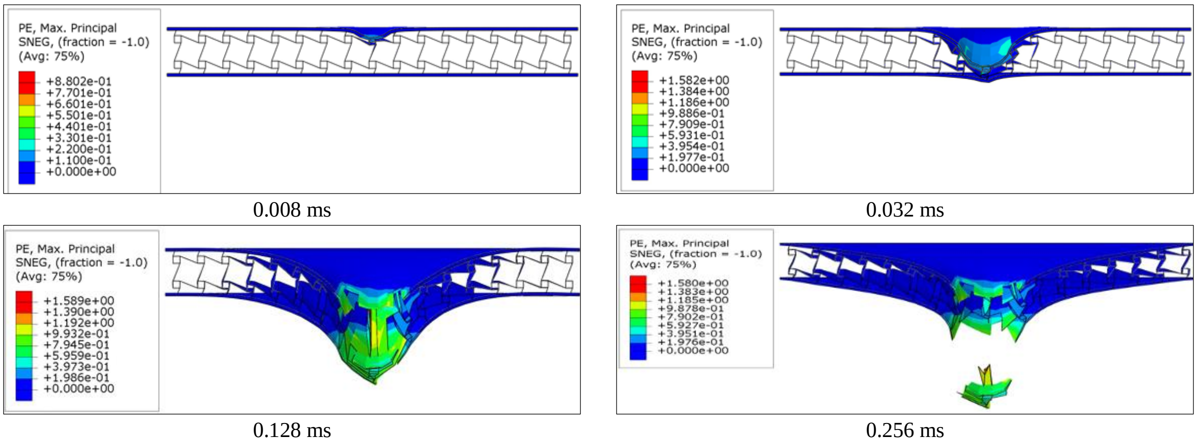

(b) Square (model 10).

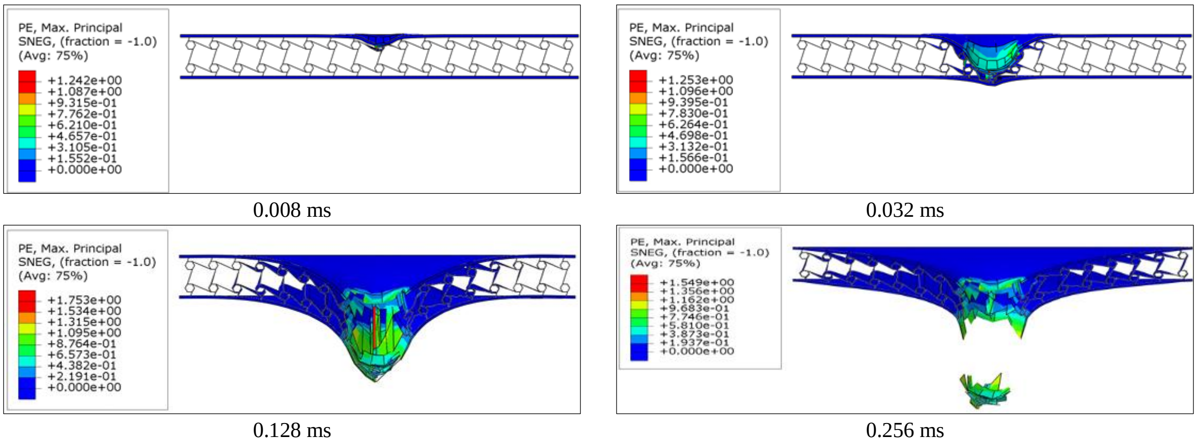

(c) Hexagon (model 11).

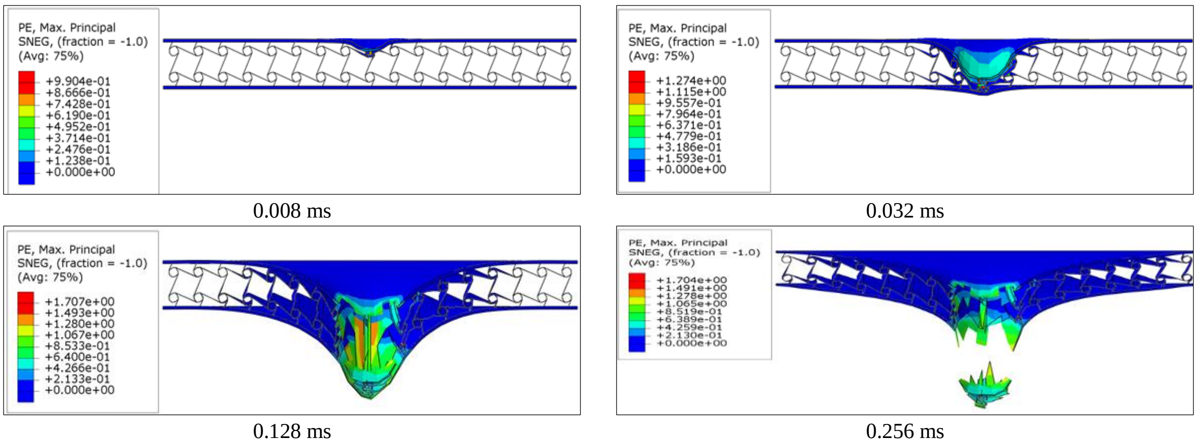

(d) Octagon (model 12).

Figure 21. Strain contours of sandwich structures with (a) circle, (b) square, (c) hexagon, and (d) octagon cores

7. Conclusions

This research examined the high-velocity impact response of tetrachiral sandwich structures whose node shapes were modified into squares, hexagons, and octagons. We also studied the response to blunt, ogive, hemispherical, and conical projectiles. The velocity used was 450 m/s. The numerical analysis method employed using ABAQUS/Explicit has been validated with previous research simulation results. The main results of this study are as follows:

- The sandwich structure material with the highest performance was Armox 500T. This material could absorb 5033.09 J of energy and reduce the projectile velocity the fastest. The stress values of the Armox 500T were the highest at 3764 MPa. Furthermore, Ti6Al4V and AISI 52100 showed similar performance results. Ti6Al4V can be an option as a protective material when considering its weight. Al 1100 had the lowest performance results regarding withstanding the impact of high-velocity projectiles.
- Several effects of the different projectile geometries were determined. It was the easiest to reduce the velocity of the blunt projectiles, meaning that the sandwich structure absorbed their energy quickly. Blunt projectiles cause failure in the structure by shear stress, while hemispherical projectiles cause failure in the front facesheet by tearing. Projectiles with a small cross-sectional area at the tip cause failure by petalling. This is because a small cross-sectional area at the tip can result in intense stress in a small area. When the structure was subjected to a conical projectile, the stress value was 3801 MPa, the highest stress of the four projectiles used.
- The circle-shaped nodes of the sandwich structure cores were modified into squares, hexagons, and octagons. The four core shapes were analyzed to determine their effects. The results show that the octagonal core had the highest performance and exceeded the performance of the circular core. However, the difference was still not large. The absorption energy value of the octagonal core was 4088.26 J, which is 2.8% higher than the absorption energy of the circular core. Meanwhile, the hexagonal core's performance was the lowest.

There were three objectives of this research: a comparison of the materials' performance, the effects of projectile geometry on the structure, and the effects of the type of core of the sandwich structure. This type of sandwich structure is intended as military vehicle armor. This study can be used as a reference in research on impact. This field of research can still be further expanded, such as by investigating buckling in cores, the effects of projectile materials, and high-velocity impact in water, among other factors.

8. Declarations

8.1. Author Contributions

Conceptualization, S.M., A.R.P., and W.W.; methodology, S.M., A.R.P., Q.T.D., and T.M.; software, Q.T.D. and T.M.; validation, S.M., A.R.P., and N.M.; formal analysis, S.M. and A.R.P.; investigation, S.M., A.R.P., and S.N.F.; resources, A.R.P. and N.M.; data curation, S.M., A.R.P., and Q.T.D.; writing—original draft preparation, S.M., A.R.P., and N.M.; writing—review and editing, S.M., A.R.P., and T.M.; visualization, W.W., N.M., and S.N.F.; supervision, A.R.P., W.W., and N.M.; project administration, A.R.P. and N.M.; funding acquisition, A.R.P. and N.M. All authors have read and agreed to the published version of the manuscript.

8.2. Data Availability Statement

The data presented in this study are available within the article.

8.3. Funding and Acknowledgement

This work was supported by the RKAT PTNBH Universitas Sebelas Maret–Year 2023, under the research scheme of “Penelitian Unggulan Terapan” (PUT-UNS), with research grant/contract No. 228/UN27.22/PT.01.03/2023. This support is gratefully acknowledged by the authors.

8.4. Conflicts of Interest

The authors declare no conflict of interest.

9. References

[1] Yu, T., & Xue, P. (2022). Utilizing plastic deformation for energy absorption. Introduction to Engineering Plasticity, 293–326. doi:10.1016/b978-0-323-98981-7.00011-7.

[2] Bao, Y., Gao, X., Wu, Y., Sun, M., & Li, G. (2021). Research progress of armor protection materials. Journal of Physics: Conference Series, 1855(1), 12035. doi:10.1088/1742-6596/1855/1/012035.

[3] Rao, C. L., Narayanamurthy, V., & Simha, K. R. Y. (2016). Ballistic Impact. Applied Impact Mechanics, 269–312. doi:10.1002/9781119241829.ch9.

[4] Li, S., Jin, F., Zhang, W., & Meng, X. (2016). Research of hail impact on aircraft wheel door with lattice hybrid structure. Journal of Physics: Conference Series, 744(1), 12102. doi:10.1088/1742-6596/744/1/012102.

[5] Borsellino, C., Calabrese, L., & Valenza, A. (2004). Experimental and numerical evaluation of sandwich composite structures. Composites Science and Technology, 64(10–11), 1709–1715. doi:10.1016/j.compscitech.2004.01.003.

[6] Ma, Q., Rejab, M. R. M., Song, Y., Zhang, X., Hanon, M. M., Abdullah, M. H., & Kumar, A. P. (2024). Effect of infill pattern of polylactide acid (PLA) 3D-printed integral sandwich panels under ballistic impact loading. Materials Today Communications, 38, 107626. doi:10.1016/j.mtcomm.2023.107626.

[7] Khalaf, W. A., & Hamzah, M. N. (2024). Experimental and numerical studies of ballistic resistance of hybrid sandwich composite body armor. Open Engineering, 14(1). doi:10.1515/eng-2022-0543.

[8] Alam, S., & Aboagye, P. (2024). Numerical Modeling on Ballistic Impact Analysis of the Segmented Sandwich Composite Armor System. Applied Mechanics, 5(2), 340–361. doi:10.3390/applmech5020020.

[9] Sadikbasha, S., & Pandurangan, V. (2023). High velocity impact response of sandwich structures with auxetic tetrachiral cores: Analytical model, finite element simulations and experiments. Composite Structures, 317, 117064. doi:10.1016/j.compstruct.2023.117064.

[10] Qin, S., Deng, X., Yang, F., & Lu, Q. (2023). Energy absorption characteristics and negative Poisson’s ratio effect of axisymmetric tetrachiral honeycombs under in-plane impact. Composite Structures, 323, 117493. doi:10.1016/j.compstruct.2023.117493.

[11] Atilla Yolcu, D., & Okutan Baba, B. (2024). Experimental investigation on impact behavior of curved sandwich composites with chiral auxetic core. Composite Structures, 329, 117749. doi:10.1016/j.compstruct.2023.117749.

[12] Pham, D. B., & Huang, S. C. (2023). A novel bio-inspired hierarchical tetrachiral structure that enhances energy absorption capacity. Journal of Mechanical Science and Technology, 37(7), 3229–3237. doi:10.1007/s12206-023-2202-y.

[13] Mohammad, Z., Gupta, P. K., & Baqi, A. (2020). Experimental and numerical investigations on the behavior of thin metallic plate targets subjected to ballistic impact. International Journal of Impact Engineering, 146, 103717. doi:10.1016/j.ijimpeng.2020.103717.

[14] Prall, D., & Lakes, R. S. (1997). Properties of a chiral honeycomb with a Poisson’s ratio of - 1. International Journal of Mechanical Sciences, 39(3), 305–307. doi:10.1016/s0020-7403(96)00025-2.

[15] Salihu, S. A., Suleiman, Y. I., Eyinavi, A. I., & Usman, A. (2019). Classification, Properties and Applications of titanium and its alloys used in aerospace, automotive, biomedical and marine industry-A Review. International Journal of Precious Engineering Research and Applications, 4(3), 23-36.

[16] Miller, W. S., Zhuang, L., Bottema, J., Wittebrood, A. J., De Smet, P., Haszler, A., & Vieregge, A. (2000). Recent development in aluminium alloys for the automotive industry. Materials Science and Engineering: A, 280(1), 37–49. doi:10.1016/s0921-5093(99)00653-x.

[17] Panda, A., Sahoo, A. K., Kumar, R., & Das, R. K. (2020). A review on machinability aspects for AISI 52100 bearing steel. Materials Today: Proceedings, 23, 617–621. doi:10.1016/j.matpr.2019.05.422.

[18] Iqbal, M. A., Senthil, K., Sharma, P., & Gupta, N. K. (2016). An investigation of the constitutive behavior of Armox 500T steel and armor piercing incendiary projectile material. International Journal of Impact Engineering, 96, 146–164. doi:10.1016/j.ijimpeng.2016.05.017.

[19] Yeter, E. (2019). Damage resistance investigation of Armox 500T and Aluminum 7075-T6 plates subjected to drop-weight and ballistic impact loads. Sakarya University Journal of Science, 23(6), 1080–1095. doi:10.16984/saufenbilder.517128.

[20] Wang, X., & Shi, J. (2013). Validation of Johnson-Cook plasticity and damage model using impact experiment. International Journal of Impact Engineering, 60, 67–75. doi:10.1016/j.ijimpeng.2013.04.010.

[21] Dong, Y., Ren, Y., Fan, S., Wang, Y., & Zhao, S. (2020). Investigation of notch-induced precise splitting of different bar materials under high-speed load. Materials, 13(11), 2461. doi:10.3390/MA13112461.

[22] Wu, B., Lin, J., Xie, A., Wang, N., Zhang, G., Zhang, J., & Dai, H. (2022). Flocking Bird Strikes on Engine Fan Blades and Their Effect on Rotor System: A Numerical Simulation. Aerospace, 9(2), 90. doi:10.3390/aerospace9020090.

[23] Ansori, D. T. A., Prabowo, A. R., Muttaqie, T., Muhayat, N., Laksono, F. B., Tjahjana, D. D. D. P., Prasetyo, A., & Kuswardi, Y. (2022). Investigation of Honeycomb Sandwich Panel Structure using Aluminum Alloy (AL6XN) Material under Blast Loading. Civil Engineering Journal (Iran), 8(5), 1046–1068. doi:10.28991/CEJ-2022-08-05-014.

[24] Nurcholis, A., Prabowo, A. R., Yaningsih, I., Muttaqie, T., Nubli, H., Huda, N., & Fajri, A. (2023). Idealized fire-structures interaction on ship and offshore building members: A benchmark study using explicit-dynamic FE approach. Procedia Structural Integrity, 48, 33–40. doi:10.1016/j.prostr.2023.07.107.

[25] Pratama, A. A., Prabowo, A. R., Muttaqie, T., Muhayat, N., Ridwan, R., Cao, B., & Laksono, F. B. (2023). Hollow tube structures subjected to compressive loading: implementation of the pitting corrosion effect in nonlinear FE analysis. Journal of the Brazilian Society of Mechanical Sciences and Engineering, 45(3), 143. doi:10.1007/s40430-023-04067-3.

[26] Do, Q. T., Xuan-Phuong, D., Tra, T. H., Tuyen, V. Van, Prabowo, A. R., & Hung, T. D. (2024). Parametric study of side collision-induced denting failures on the ultimate strength of a handy-size containership under vertical bending. Ocean Engineering, 309, 118534. doi:10.1016/j.oceaneng.2024.118534.

[27] Wiranto, I. B., Saraswati, S. O., Alfikri, I. R., Chairunnisa, C., Megawanto, F. C., Adhynugraha, M. I., & Majid, N. C. (2024). Effect of Boundary Condition on Numerical Study of UAV Composite Skin Panels Under Dynamic Impact Loading. Mekanika: Majalah Ilmiah Mekanika, 23(1), 22. doi:10.20961/mekanika.v23i1.77875.

[28] Nurcholis, A., Prabowo, A. R., Muhayat, N., Yaningsih, I., Tjahjana, D. D. D. P., Jurkovič, M., Sohn, J. M., Adiputra, R., Hanif, M. I., & Ridwan, R. (2024). Performances of the sandwich panel structures under fire accident due to hydrogen leaks: Consideration of structural design and environment factor using FE analysis. Curved and Layered Structures, 11(1), 20240005. doi:10.1515/cls-2024-0005.

[29] Naufal, A. M., Prabowo, A. R., Muttaqie, T., Hidayat, A., Purwono, J., Adiputra, R., Akbar, H. I., & Smaradhana, D. F. (2024). Characterization of sandwich materials – Nomex-Aramid carbon fiber performances under mechanical loadings: Nonlinear FE and convergence studies. Reviews on Advanced Materials Science, 63(1), 20230177. doi:10.1515/rams-2023-0177.

[30] Sahraei, A., Pezeshky, P., Sasibut, S., Rong, F., & Mohareb, M. (2022). Finite element formulation for the dynamic analysis of shear deformable thin-walled beams. Thin-Walled Structures, 173, 108989. doi:10.1016/j.tws.2022.108989.

[31] Prabowo, A. R., Ridwan, R., Braun, M., Song, S., Ehlers, S., Firdaus, N., & Adiputra, R. (2023). Comparative study of shell element formulations as NLFE parameters to forecast structural crashworthiness. Curved and Layered Structures, 10(1), 20220217. doi:10.1515/cls-2022-0217.

[32] Prabowo, A. R., Ridwan, R., Tuswan, T., Smaradhana, D. F., Cao, B., & Baek, S. J. (2024). Crushing resistance on the metal-based plate under impact loading: A systematic study on the indenter radius influence in grounding accident. Applications in Engineering Science, 18, 100177. doi:10.1016/j.apples.2024.100177.

[33] Prabowo, A. R., Cahyono, S. I., & Sohn, J. M. (2019). Crashworthiness assessment of thin-walled double bottom tanker: A variety of ship grounding incidents. Theoretical and Applied Mechanics Letters, 9(5), 320–327. doi:10.1016/j.taml.2019.05.002.

[34] Främby, J., Fagerström, M., & Karlsson, J. (2020). An adaptive shell element for explicit dynamic analysis of failure in laminated composites Part 1: Adaptive kinematics and numerical implementation. Engineering Fracture Mechanics, 240, 107288. doi:10.1016/j.engfracmech.2020.107288.

[35] Del Priore, E., & Lampani, L. (2024). A methodology for applying isogeometric inverse finite element method to the shape sensing of stiffened thin-shell structures. Thin-Walled Structures, 199, 111837. doi:10.1016/j.tws.2024.111837.

[36] Ridwan, R., Sudarno, S., Nubli, H., Chasan, A., Istanto, I., & Pratama, P. S. (2023). Numerical Analysis of Openings in Stiffeners under Impact Loading: Investigating Structural Response and Failure Behavior. Mekanika: Majalah Ilmiah Mekanika, 22(2), 115. doi:10.20961/mekanika.v22i2.76774.

[37] Carvalho, H., Ridwan, R., Sudarno, S., Prabowo, A. R., Bae, D. M., & Huda, N. (2023). Failure criteria in crashworthiness analysis of ship collision and grounding using FEA: Milestone and development. Mekanika: Majalah Ilmiah Mekanika, 22(1), 30. doi:10.20961/mekanika.v22i1.70959.

[38] Kim, S. J., Taimuri, G., Kujala, P., Conti, F., Le Sourne, H., Pineau, J. P., Looten, T., Bae, H., Mujeeb-Ahmed, M. P., Vassalos, D., Kaydihan, L., & Hirdaris, S. (2022). Comparison of numerical approaches for structural response analysis of passenger ships in collisions and groundings. Marine Structures, 81, 103125. doi:10.1016/j.marstruc.2021.103125.

[39] Prabowo, A. R., Muttaqie, T., Sohn, J. M., & Bae, D. M. (2018). Nonlinear analysis of inter-island roro under impact: Effects of selected collision's parameters on the crashworthy double-side structures. Journal of the Brazilian Society of Mechanical Sciences and Engineering, 40(5), 248. doi:10.1007/s40430-018-1169-6.